



## Characterizing the tropospheric ozone response to methane emission controls and the benefits to climate and air quality

Arlene M. Fiore,<sup>1</sup> J. Jason West,<sup>2,3,4</sup> Larry W. Horowitz,<sup>1</sup> Vaishali Naik,<sup>3</sup> and M. Daniel Schwarzkopf<sup>1</sup>

Received 12 July 2007; revised 2 November 2007; accepted 12 December 2007; published 30 April 2008.

[1] Reducing methane (CH<sub>4</sub>) emissions is an attractive option for jointly addressing climate and ozone (O<sub>3</sub>) air quality goals. With multidecadal full-chemistry transient simulations in the MOZART-2 tropospheric chemistry model, we show that tropospheric O<sub>3</sub> responds approximately linearly to changes in CH<sub>4</sub> emissions over a range of anthropogenic emissions from 0–430 Tg CH<sub>4</sub> a<sup>-1</sup> (0.11–0.16 Tg tropospheric O<sub>3</sub> or ~11–15 ppt global mean surface O<sub>3</sub> decrease per Tg a<sup>-1</sup> CH<sub>4</sub> reduced). We find that neither the air quality nor climate benefits depend strongly on the location of the CH<sub>4</sub> emission reductions, implying that the lowest cost emission controls can be targeted. With a series of future (2005–2030) transient simulations, we demonstrate that cost-effective CH<sub>4</sub> controls would offset the positive climate forcing from CH<sub>4</sub> and O<sub>3</sub> that would otherwise occur (from increases in NO<sub>x</sub> and CH<sub>4</sub> emissions in the baseline scenario) and improve O<sub>3</sub> air quality. We estimate that anthropogenic CH<sub>4</sub> contributes 0.7 Wm<sup>-2</sup> to climate forcing and ~4 ppb to surface O<sub>3</sub> in 2030 under the baseline scenario. Although the response of surface O<sub>3</sub> to CH<sub>4</sub> is relatively uniform spatially compared to that from other O<sub>3</sub> precursors, it is strongest in regions where surface air mixes frequently with the free troposphere and where the local O<sub>3</sub> formation regime is NO<sub>x</sub>-saturated. In the model, CH<sub>4</sub> oxidation within the boundary layer (below ~2.5 km) contributes more to surface O<sub>3</sub> than CH<sub>4</sub> oxidation in the free troposphere. In NO<sub>x</sub>-saturated regions, the surface O<sub>3</sub> sensitivity to CH<sub>4</sub> can be twice that of the global mean, with >70% of this sensitivity resulting from boundary layer oxidation of CH<sub>4</sub>. Accurately representing the NO<sub>x</sub> distribution is thus crucial for quantifying the O<sub>3</sub> sensitivity to CH<sub>4</sub>.

**Citation:** Fiore, A. M., J. J. West, L. W. Horowitz, V. Naik, and M. D. Schwarzkopf (2008), Characterizing the tropospheric ozone response to methane emission controls and the benefits to climate and air quality, *J. Geophys. Res.*, 113, D08307, doi:10.1029/2007JD009162.

### 1. Introduction

[2] Methane (CH<sub>4</sub>) emission controls are currently receiving attention as a viable low-cost strategy for abating surface ozone (O<sub>3</sub>) pollution while simultaneously slowing greenhouse warming [Hansen *et al.*, 2000; Fiore *et al.*, 2002a; Dentener *et al.*, 2005; EMEP, 2005; West and Fiore, 2005; West *et al.*, 2006]. In the presence of nitrogen oxides (NO<sub>x</sub>), tropospheric CH<sub>4</sub> oxidation leads to the formation of O<sub>3</sub> [Crutzen, 1973]. Over the last century, global background O<sub>3</sub> concentrations have risen by at least a factor of two, due mainly to increases in CH<sub>4</sub> and NO<sub>x</sub> emissions

[e.g., Marenco *et al.*, 1994; Wang and Jacob, 1998]. Here, we characterize the response of tropospheric O<sub>3</sub> to controls on CH<sub>4</sub> emissions, analyze the dominant processes determining the distribution of this response, and quantify the resulting benefits to air quality and climate.

[3] With a lifetime of approximately a decade, CH<sub>4</sub> is fairly well-mixed in the atmosphere. Sources of atmospheric CH<sub>4</sub> include wetlands, ruminants, energy, rice agriculture, landfills, wastewater, biomass burning, oceans, and termites. Anthropogenic emissions are estimated to contribute at least 60% to total CH<sub>4</sub> emissions, with individual studies reporting a range of 500 to 610 Tg a<sup>-1</sup> for total CH<sub>4</sub> emissions [Denman *et al.*, 2007]. The dominant CH<sub>4</sub> sink is reaction with the hydroxyl radical (OH) in the troposphere. If sufficient quantities of NO<sub>x</sub> are available, CH<sub>4</sub> oxidation produces O<sub>3</sub> via reactions of peroxy radicals with NO<sub>x</sub>. In a low-NO<sub>x</sub> environment, formation of methyl hydroperoxide (CH<sub>3</sub>OOH) suppresses O<sub>3</sub> production and may provide a net O<sub>3</sub> sink. In an extremely low-NO<sub>x</sub> environment, CH<sub>4</sub> oxidation may also decrease O<sub>3</sub> levels by HO<sub>2</sub> reacting preferentially with O<sub>3</sub> rather than with NO. Under present-day tropospheric conditions, however, Spivakovsky *et al.*

<sup>1</sup>NOAA Geophysical Fluid Dynamics Laboratory, Princeton, New Jersey, USA.

<sup>2</sup>Atmospheric and Oceanic Sciences Program, Princeton University, Princeton, New Jersey, USA.

<sup>3</sup>Woodrow Wilson School of Public and International Affairs, Princeton University, Princeton, New Jersey, USA.

<sup>4</sup>Now at University of North Carolina at Chapel Hill, Chapel Hill, North Carolina, USA.

[2000] show that  $\text{HO}_2 + \text{NO}$  is more important than  $\text{HO}_2 + \text{O}_3$  globally as a source of OH (their Figure 10), implying that increases in  $\text{CH}_4$  abundances should yield a net global increase in the tropospheric  $\text{O}_3$  burden, as has been reported in prior modeling studies [e.g., Prather *et al.*, 2001]. Previously,  $\text{CH}_4$  and  $\text{NO}_x$  emission reductions have been shown to be the most effective means of lowering tropospheric  $\text{O}_3$ : reductions in anthropogenic  $\text{NO}_x$  emissions decrease surface  $\text{O}_3$  in polluted source regions by up to four times more than equivalent percentage reductions in anthropogenic  $\text{CH}_4$  emissions, while  $\text{CH}_4$  reductions have a stronger impact on the tropospheric  $\text{O}_3$  burden, and a similar influence to  $\text{NO}_x$  on global average surface  $\text{O}_3$  concentrations [Fiore *et al.*, 2002a; West *et al.*, 2008].

[4] To date, most chemical transport model (CTM) studies have applied a uniform  $\text{CH}_4$  mixing ratio to avoid the computational expense of multidecadal simulations required for  $\text{CH}_4$  to reach a steady state [e.g., Prather *et al.*, 2001; Stevenson *et al.*, 2006]. We have previously adopted this approach to evaluate the benefits to human health, agriculture, and commercial forests resulting from lower  $\text{O}_3$  due to  $\text{CH}_4$  emission reductions [West and Fiore, 2005; West *et al.*, 2006]. In such simulations, termed “steady state” in our analysis below, the uniform  $\text{CH}_4$  mixing ratio is adjusted to reflect a desired  $\text{CH}_4$  emission change, accounting for the non-linear feedback of  $\text{CH}_4$  on its own lifetime through OH [Prather, 1996; Prather *et al.*, 2001]. Since the relationship between  $\text{CH}_4$  emissions and  $\text{CH}_4$  concentrations is non-linear, it is important to assess the degree to which this non-linearity affects the accuracy of estimates obtained by scaling results (e.g., changes in  $\text{O}_3$  concentrations) from one  $\text{CH}_4$  perturbation to another.

[5] In Figure 1, we compile estimates of the response of tropospheric  $\text{O}_3$  to changes in  $\text{CH}_4$  emissions from several global CTMs in the literature, to investigate whether changes in  $\text{O}_3$  scale linearly with changes in  $\text{CH}_4$  emissions. We include results from transient, full-chemistry simulations [Dentener *et al.*, 2005], from “steady state” simulations with a uniform, fixed  $\text{CH}_4$  concentration [Wang and Jacob, 1998; Prather *et al.*, 2001; Fiore *et al.*, 2002a; West *et al.*, 2006, 2008], and from a hybrid modeling approach [Shindell *et al.*, 2005]. Despite variations in the simulation type, the total  $\text{CH}_4$  emissions, the anthropogenic fraction of  $\text{CH}_4$  emissions, and the emissions of other species that affect OH, Figure 1 shows that the tropospheric  $\text{O}_3$  burden responds roughly linearly to changes in anthropogenic  $\text{CH}_4$  emissions across the models. Estimates from the individual studies range from 0.12–0.16 Tg tropospheric  $\text{O}_3$  per  $\text{Tg a}^{-1}$  change in  $\text{CH}_4$  emissions. Although the feedback between  $\text{CH}_4$  and OH will cause the  $\text{CH}_4$  concentration to respond in a strongly non-linear manner for sufficiently large increases in  $\text{CH}_4$  emissions, the relationship is approximately linear for the range of emission perturbations considered in Figure 1, corroborating earlier results derived from theory and applied in a one-box model [Prather, 1996]. We further estimate from the published studies in Figure 1 that anthropogenic  $\text{CH}_4$  currently contributes  $\sim 50$  Tg to the annual mean tropospheric  $\text{O}_3$  burden, and  $\sim 5$  ppb to global mean surface  $\text{O}_3$  (based on the subset of models reporting changes in surface  $\text{O}_3$  [Fiore *et al.*, 2002a; Dentener *et al.*, 2005; West *et al.*, 2006]).

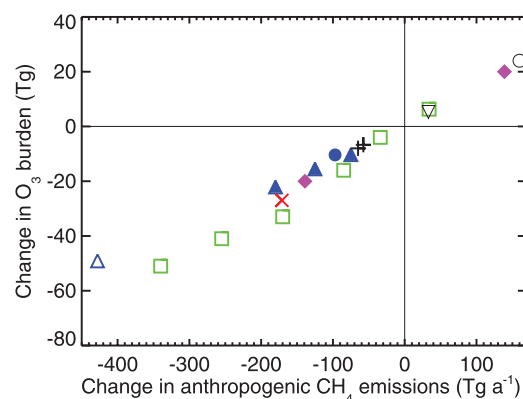


**Figure 1.** The change in tropospheric  $\text{O}_3$  burden (Tg) as a function of the change in anthropogenic  $\text{CH}_4$  emissions ( $\text{Tg a}^{-1}$ ), compiled from modeling studies in the literature encompassing a range of modeling approaches: (1) full-chemistry, transient simulations (pink filled diamonds: TM3 [Dentener *et al.*, 2005]; blue filled circle: RGLOB-BASE in this work; blue filled triangles: 2030 results from future scenarios A, B, and C in this work), (2) steady state simulations in which a uniform, fixed  $\text{CH}_4$  concentration is adjusted to reflect a change in  $\text{CH}_4$  emissions (red x: GEOS-Chem [Fiore *et al.*, 2002a]; black upside down triangle: Recommended based on IPCC TAR models, with the  $\text{O}_3$  burden change reduced by 25% to correct for the inclusion of stratospheric  $\text{O}_3$  in the reported results [Prather *et al.*, 2001]; black +: MOZART-2 [West *et al.*, 2006, 2008]; open black circle: addition of  $\text{CH}_4$  to the pre-industrial atmosphere in a global CTM [Wang and Jacob, 1998]; open blue triangle:  $\text{CH}_4$ -700 simulation in this work), and (3) a hybrid approach where the initial  $\text{CH}_4$  trends from a transient simulation were extrapolated exponentially using the model’s  $\text{CH}_4$  perturbation time of 12.6 years, followed by 5 additional years of simulation (green squares: GISS [Shindell *et al.*, 2005; personal communication, 2006]). All blue symbols (from RGLOB-BASE and the differences of the 2030 A, B, C,  $\text{CH}_4$ -700 and 2030 CLE simulations) denote the  $\text{O}_3$  burden change adjusted to steady state as described in section 3. The two left-most points depict simulations in which anthropogenic  $\text{CH}_4$  emissions are eliminated.

[6] Designing effective  $\text{CH}_4$  controls to combat  $\text{O}_3$  air pollution requires knowledge of the magnitude and spatial pattern of the surface  $\text{O}_3$  response to changes in  $\text{CH}_4$  emissions. The sensitivity of  $\text{O}_3$  to changes in  $\text{CH}_4$  should depend on the emission ratio of  $\text{NO}_x$  to non-methane volatile organic compounds (NMVOC) and carbon monoxide (CO), which affects the abundance of OH [Wang and Jacob, 1998; West *et al.*, 2006]. Here, we apply the global MOZART-2 CTM to characterize the  $\text{O}_3$  response to  $\text{CH}_4$  emission changes both with and without changes in emissions of other species ( $\text{NO}_x$ , CO and NMVOC; sections 3 and 4). We then examine the processes contributing to the regional pattern of the  $\text{O}_3$  response to  $\text{CH}_4$  (section 5), and identify any dependence of this response on the geographical location of the  $\text{CH}_4$  source (section 6). Finally, we quantify the global and regional air quality (section 7) and

**Table 1.** Description of MOZART-2 Simulations

Simulation Name	CH <sub>4</sub> Emissions or Mixing Ratio	Non-CH <sub>4</sub> O <sub>3</sub> Precursor Emissions	NCEP years
Transient simulations			
BASE	BASE (see Table 2)	BASE	1990–2004, recycled once
RGLOB	BASE with anthropogenic emissions <sup>a</sup> reduced by 97 Tg a <sup>-1</sup>		1990–2004, recycled once
RASIA	BASE with anthropogenic emissions <sup>a</sup> in Asia set to zero (-97 Tg a <sup>-1</sup> )		1990–2000 <sup>d</sup>
CLE <sup>b</sup>	CLE 2005–2030 (Table 2; Figure 2a)	CLE	2000–2004, recycled five times for the 2005–2030 period
A	CLE 2005–2030 with 75 Tg a <sup>-1</sup> decrease <sup>c</sup> by 2030 (Figure 2a)		
B	CLE 2005–2030 with 125 Tg a <sup>-1</sup> decrease <sup>c</sup> by 2030 (Figure 2a)		
C	CLE 2005–2030 with 180 Tg a <sup>-1</sup> decrease <sup>c</sup> by 2030 (Figure 2a)		
Steady state simulations			
GLOB1760	[CH <sub>4</sub> ] = 1760 ppb	BASE	2000
GLOB1460	[CH <sub>4</sub> ] = 1460 ppb		
FT1460	[CH <sub>4</sub> ] = 1460 ppb above 724 hPa; [CH <sub>4</sub> ] = 1760 ppb elsewhere		
PBL1460	[CH <sub>4</sub> ] = 1760 ppb above 724 hPa; [CH <sub>4</sub> ] = 1460 ppb elsewhere		
CH <sub>4</sub> -700	[CH <sub>4</sub> ] = 700 ppb	CLE year 2030	

<sup>a</sup>Anthropogenic emissions are as defined in Table 2 but exclude agricultural waste burning. The 97 Tg a<sup>-1</sup> reduction in BASE is applied to the anthropogenic emissions as a globally uniform decrease of 39%.

<sup>b</sup>Current Legislation Scenario [Dentener *et al.*, 2005].

<sup>c</sup>The anthropogenic (industrial plus agricultural) CLE CH<sub>4</sub> emissions were scaled to the desired emission reduction according to the spatial pattern of the difference between CH<sub>4</sub> emissions in the CLE and “Maximum Technologically Feasible Reduction” (MFR) scenarios in 2030 from Dentener *et al.* [2005].

<sup>d</sup>The RASIA simulation was stopped after 11 years since there was little difference in the O<sub>3</sub> response from that in RGLOB.

radiative forcing (section 8) impacts that could be attained via CH<sub>4</sub> controls from 2005 to 2030.

## 2. Methane Simulations

[7] We apply the MOZART-2 global model of tropospheric chemistry [Horowitz *et al.*, 2003] to assess the response of O<sub>3</sub> to changes in CH<sub>4</sub> emissions. Table 1 provides a summary of the twelve simulations used in our study, which are described in detail below. We first consider sustained CH<sub>4</sub> emission reductions in transient simulations in which other emissions are held fixed at present-day values (section 2.1) in order to diagnose the CH<sub>4</sub>-OH feedback factor in our model and to characterize the tropospheric O<sub>3</sub> response to CH<sub>4</sub> emission controls. We then apply CH<sub>4</sub> controls phased in between 2005 and 2030 along three different trajectories, relative to a baseline future emission scenario in which emissions of CH<sub>4</sub> and other O<sub>3</sub> precursors change (section 2.2). These future scenarios in which CH<sub>4</sub> controls are implemented in a more plausible manner allow us both to quantify the climate and air quality benefits that could be attained via different policy options and to examine the extent to which these benefits can be scaled from one CH<sub>4</sub> control trajectory to another. Finally, we employ “steady state” simulations (section 2.3) to examine the relative impact of CH<sub>4</sub> oxidation in the free troposphere versus in the boundary layer on surface O<sub>3</sub>, and to quantify the total contribution of anthropogenic CH<sub>4</sub> to tropospheric O<sub>3</sub>. All simulations are driven by meteorological fields from the NCEP reanalysis [Kalnay *et al.*, 1996] at a horizontal resolution of 1.9° × 1.9° with 28 vertical levels. We update the isoprene nitrate chemistry, from the 8% yield [Carter and Atkinson, 1996] used by Horowitz *et al.* [2003] to 12% [Sprengnether *et al.*, 2002], and treat isoprene nitrates as a NO<sub>x</sub> sink [e.g., Chen *et al.*, 1998]; this modification reduces the positive bias in the MOZART-2 surface O<sub>3</sub> simulation

[Murazaki and Hess, 2006] as discussed further in section 2.4. Our simulations focus exclusively on the role of changes in O<sub>3</sub> precursor emissions and do not include any impacts resulting from future changes in climate.

### 2.1. Transient Simulations of Sustained CH<sub>4</sub> Reductions

[8] We conduct three full-chemistry transient simulations beginning in 1990, with emissions of all O<sub>3</sub> precursors, except for CH<sub>4</sub> (and the lightning NO<sub>x</sub> source which is tied to the meteorology as by Horowitz *et al.* [2003]), held constant. In the first simulation (BASE), we maintain CH<sub>4</sub> emissions at 1990 levels. The BASE CH<sub>4</sub> emissions (Table 2) include 308 Tg a<sup>-1</sup> from anthropogenic sources [Olivier *et al.*, 1996, 1999] and 25 Tg a<sup>-1</sup> from biomass burning [Horowitz *et al.*, 2003]. We uniformly increase the global wetland emissions from Horowitz *et al.* [2003] by 40% to 204 Tg a<sup>-1</sup> on the basis of recent estimates [Wang *et al.*, 2004]. The 1990–2004 winds are recycled to complete 30-year simulations.

[9] Since we wish to investigate the sensitivity of O<sub>3</sub> to the geographical location of CH<sub>4</sub> emissions, we conduct two additional simulations, in both of which global anthropogenic CH<sub>4</sub> emissions are decreased by the same magnitude. In one simulation (RASIA), we set Asian (India, East Asia, and Southeast Asia as defined by Naik *et al.* [2005]) anthropogenic CH<sub>4</sub> emissions (97 Tg a<sup>-1</sup>; excluding agricultural waste burning) to zero. In the other simulation (RGLOB), we obtain the same 97 Tg a<sup>-1</sup> reduction by uniformly decreasing CH<sub>4</sub> emissions from all anthropogenic sectors (except for agricultural waste burning) by 39%. The decrease of 97 Tg a<sup>-1</sup> corresponds to an 18% reduction in total global CH<sub>4</sub> emissions.

[10] The model includes the major CH<sub>4</sub> loss mechanism of reaction with tropospheric OH (450–480 Tg a<sup>-1</sup> in BASE; range reflects variability over the 15 years), as well

**Table 2.** Methane Emissions ( $\text{Tg CH}_4 \text{ a}^{-1}$ ) Used in This Study

Year	BASE	Current Legislation (CLE)			
	1990s	2005	2010	2020	2030
Anthropogenic	308 <sup>a</sup>	332 <sup>d</sup>	364 <sup>d</sup>	397 <sup>d</sup>	428 <sup>d</sup>
Natural <sup>b</sup>	214	222	222	222	222
Biomass burning <sup>c</sup>	25	23	23	23	23
Total	547	577	609	642	673

<sup>a</sup>Emissions in the BASE simulation include energy use, landfills, wastewater, rice, ruminants, and agricultural waste burning from the EDGAR v2.0 inventory [Olivier et al., 1996, 1999] as described in Horowitz et al. [2003].

<sup>b</sup>Includes  $10 \text{ Tg a}^{-1}$  from oceans. The distribution and seasonality of the wetland emissions are from Horowitz et al. [2003] in BASE, and from Wang et al. [2004] in CLE.

<sup>c</sup>For BASE, biomass burning of savannas and forests is from Horowitz et al. [2003]. The CLE simulations use biomass burning from the Global Fire Emissions Database (GFEDv1) climatology for 1997–2002 [Van der Werf et al., 2003].

<sup>d</sup>Includes anthropogenic  $\text{CH}_4$  emissions separated into agricultural and industrial sectors as specified in the CLE inventory [Dentener et al., 2005].

as minor losses to soils ( $20 \text{ Tg a}^{-1}$  in BASE, imposed via a deposition velocity) and in the stratosphere ( $50\text{--}70 \text{ Tg a}^{-1}$  in BASE). Methane losses in the stratosphere by reaction with OH and  $\text{O}(^1\text{D})$  are modeled explicitly, and loss by reaction with chlorine is accounted for by prescribing the  $\text{CH}_4$  concentration in the upper two model levels (above 14 hPa) to zonally and monthly averaged values from the middle atmosphere model Study of Transport and Chemical Reactions in the Stratosphere (STARS) [Brasseur et al., 1997] as described by Horowitz et al. [2003]. For the 30-year RGLOB simulation, these climatological values were decreased by 18% in an effort to account for the decrease in stratospheric concentrations that would result from the reduction in  $\text{CH}_4$  emissions.

[11] Emissions of  $\text{O}_3$  precursors besides  $\text{CH}_4$  from all sources are as described by Horowitz et al. [2003] except for  $\text{NO}_x$  emissions from ships, which have been removed on the basis that their inclusion likely leads to unrealistically high  $\text{NO}_x$  concentrations in the marine boundary layer in global models that neglect the rapid  $\text{NO}_x$  destruction recently observed to occur inside the ship plume [Kasibhatla et al., 2000; Chen et al., 2005]. Eyring et al. [2007], however, found that the ensemble mean oceanic  $\text{NO}_x$  concentrations from 10 global models that included ship emissions fell within the range of a wider observational data set than that used by Kasibhatla et al. [2000]. They point out, however, that the modeled difference from including versus excluding ship emissions is too weak to be accurately evaluated with available measurements [Eyring et al., 2007]. While the impact of ship  $\text{NO}_x$  emissions on the oceanic atmosphere is still uncertain, Eyring et al. [2007] show that the ship  $\text{NO}_x$  emissions in the year 2000 CLE inventory (which we include in our transient future scenarios described below) decrease the  $\text{CH}_4$  lifetime in the models by 0.13 years (10-model ensemble mean). We further discuss the impact of ship  $\text{NO}_x$  emissions in the context of our results in section 4.

## 2.2. Transient Future Scenarios

[12] In order to project the impact of  $\text{CH}_4$  emission controls on future air quality and climate, we conduct a second set of transient simulations, using the “Current Legislation” (CLE) scenario for 2000 to 2030 as a baseline

[Cofala et al., 2005; Dentener et al., 2005]. This scenario incorporates existing emission control legislation on the traditional air pollutants  $\text{NO}_x$ , CO, and NMVOC around the globe to describe the evolution of  $\text{O}_3$  precursors [Dentener et al., 2005] and is thus more optimistic than the widely used IPCC SRES scenarios [Nakicenovic et al., 2000]. Simulations applying 2000 and 2030 CLE emissions, but with uniform  $\text{CH}_4$  abundances, were previously conducted with MOZART-2 and analyzed as part of the multi-model ACCENT Photocomp Experiment 2 [Dentener et al., 2006a, 2006b; Shindell et al., 2006; Stevenson et al., 2006; van Noije et al., 2006].

[13] Here, we conduct transient simulations for 2000–2030 following the CLE scenario, with the period 2000–2004 used for spin-up. We adopt the approach of Dentener et al. [2005], interpolating the CLE emissions provided for the years 2000, 2010, 2020, and 2030 to obtain annual emissions; Table 2 shows the growth of  $\text{CH}_4$  emissions from 2005 to 2030. Between 2005 and 2030, baseline CLE anthropogenic emissions of  $\text{CH}_4$ ,  $\text{NO}_x$ , CO, and NMVOC change by +29% ( $+96 \text{ Tg CH}_4 \text{ a}^{-1}$ ), +19% ( $+5.3 \text{ Tg N a}^{-1}$ ), –10% ( $-44 \text{ Tg CO a}^{-1}$ ), and +3% ( $+3 \text{ Tg C a}^{-1}$ ), respectively. Aircraft emissions are assumed to grow linearly, from 0.8 to  $1.7 \text{ Tg N a}^{-1}$  ( $\text{NO}_x$ ) and 1.7 to  $3.7 \text{ Tg a}^{-1}$  CO, as recommended for the ACCENT Photocomp Experiment 2 simulations for 2000 and 2030 [Stevenson et al., 2006], based on the IS92a scenario [Henderson et al., 1999]. Biomass burning emissions are taken from the 1997–2002 GFED v.1 biomass burning climatology [Van der Werf et al., 2003], vertically distributed following the recommendations for the ACCENT Photocomp Experiment 2, and assumed constant into the future. Wetland emissions are based upon the seasonal and spatial distribution from Wang et al. [2004] as described by Fiore et al. [2006], but here we reduce  $\text{CH}_4$  emissions from swamps by  $12 \text{ Tg a}^{-1}$ , in an effort to reduce the positive tropical bias as compared to the NOAA GMD observations found in that study. The NCEP meteorology for 2000–2004 is recycled every 5 years to allow for interannual variability in the  $\text{O}_3$  response to  $\text{CH}_4$ ; these years were chosen on the basis of our previous work showing that the meteorology during these years yields a relatively constant  $\text{CH}_4$  lifetime when emissions are held constant [Fiore et al., 2006], and thus should minimize discontinuous changes in the  $\text{CH}_4$  sink by tropospheric OH when the winds are recycled. Losses of  $\text{CH}_4$  transported into the stratosphere are treated as described in section 2.1 with the exception of the prescribed climatology in the upper 2 model levels; we instead relax the model  $\text{CH}_4$  concentrations in these levels to zero with a six month lifetime to account for  $\text{CH}_4$  loss by reaction with chlorine. The six month lifetime retains the same present-day stratospheric loss rate as in BASE, while allowing the stratospheric  $\text{CH}_4$  sink to adjust to changes in the atmospheric burden resulting from changes in emissions. Additional model updates in these simulations include an increase of the  $\text{O}(^1\text{D}) + \text{N}_2$  rate constant [Ravishankara et al., 2002] and the inclusion of near-infrared photolysis of  $\text{HO}_2\text{NO}_2$  [Roehl et al., 2002].

[14] We conduct three simulations using  $\text{CH}_4$  reduction scenarios relative to the baseline CLE scenario beginning in 2006 (Figure 2). Compared to the 17% increase in total  $\text{CH}_4$  emissions in the baseline CLE scenario between 2005 and

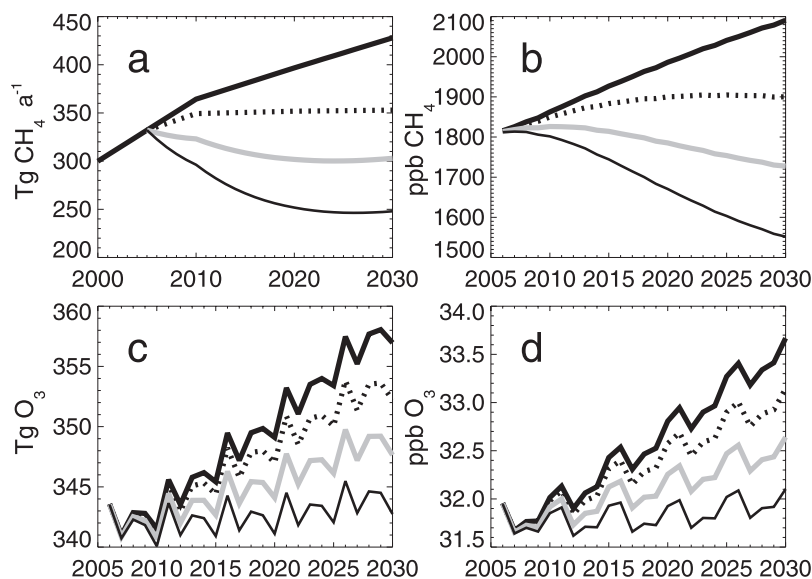


**Figure 2.** (a) Anthropogenic  $\text{CH}_4$  emissions ( $\text{Tg a}^{-1}$ ), (b) annual mean surface  $\text{CH}_4$  mixing ratios in dry air (ppb) (c) annual mean tropospheric  $\text{O}_3$  burden (Tg), and (d) 8-h daily maximum (MDA8)  $\text{O}_3$  concentrations (ppb) under the CLE scenario (thick black line), and following  $\text{CH}_4$  control scenarios A (dotted line), B (grey line), and C (thin black line), described in section 2.2. The 150 ppb  $\text{O}_3$  chemical tropopause in 2005 is used to calculate the tropospheric  $\text{O}_3$  burden.

2030 (Table 2), emissions increase by only 4% in scenario A and decline by 5% and 15% in scenarios B and C, respectively, over this period. Further details on the development of these scenarios are provided by J. J. West et al. [Management of tropospheric ozone by reducing methane emissions: Comparison of abatement costs and global mortality benefits under future methane abatement scenarios, manuscript in preparation, 2008], along with an estimate of the associated costs and public health benefits. Briefly, scenario A corresponds to an 18% ( $75 \text{ Tg a}^{-1}$ ) decrease in global anthropogenic  $\text{CH}_4$  emissions (defined as the agricultural and industrial sectors provided in the CLE inventory) relative to the projected CLE emissions in 2030. Scenario B involves a 29% ( $125 \text{ Tg a}^{-1}$ ) decrease in global anthropogenic  $\text{CH}_4$  emissions in 2030, slightly less than the reductions achieved in the IIASA Maximum Feasible Reductions (MFR) scenario versus CLE in 2030, and should be cost-effective with available technologies at a marginal cost of approximately \$315 per ton  $\text{CH}_4$  (\$15 per ton  $\text{CO}_2$  equivalent). Scenario C requires development of additional control technologies, likely in the large agricultural sector, to achieve a 42% ( $180 \text{ Tg a}^{-1}$ ) reduction of global anthropogenic  $\text{CH}_4$  emissions by 2030.

### 2.3. Steady State Simulations

[15] We conduct four “steady state” simulations to diagnose the relative contribution to surface  $\text{O}_3$  from  $\text{CH}_4$  oxidation in the free troposphere versus boundary layer (Table 1). In these simulations, we use the BASE emissions for all species besides  $\text{CH}_4$ , but fix atmospheric  $\text{CH}_4$  mixing ratios to (1) 1760 ppb everywhere (GLOB1760 simulation), (2) 1460 ppb everywhere (GLOB1460), (3) 1460 ppb in the boundary layer and 1760 ppb elsewhere (PBL1460), and (4) 1760 ppb in the boundary layer and 1460 ppb in the free troposphere (FT1460). The model level centered at 750 hPa

(top edge at 724 hPa or  $\sim 2.5$  km) is included as the uppermost level within the boundary layer. These four simulations were spun up beginning in May 1999 and results are examined for the year 2000. We conduct an additional simulation in which we use the CLE 2030 emissions for non- $\text{CH}_4$   $\text{O}_3$  precursors and fix  $\text{CH}_4$  concentrations uniformly to the 700 ppb pre-industrial level, in order to quantify the total contribution of anthropogenic  $\text{CH}_4$  to tropospheric  $\text{O}_3$  in the year 2030.

### 2.4. Model Evaluation

[16] The annual mean latitudinal bias in our  $\text{CH}_4$  simulations (BASE and CLE) is compared to the NOAA GMD observations [Dlugokencky et al., 2005] for the year 2004 in Figure 3. For both simulations, the simulated  $\text{CH}_4$  concentrations are within 5% of the observations at all locations. The BASE simulation has previously been shown to capture much of the observed  $\text{CH}_4$  rise in the early 1990s, along with the flattening in the late 1990s [Fiore et al., 2006]. A major shortcoming in BASE is the 50% overestimate of the mean 2004 gradient from the South Pole to Alert (195 ppb versus 127 ppb observed). This overestimate is corrected in the CLE simulation (121 ppb gradient) largely due to the use of the Wang et al. [2004] wetland distribution, which also improves the seasonal cycles in the model at northern hemispheric sites [Fiore et al., 2006]. As we show in section 4, the  $\text{O}_3$  response to  $\text{CH}_4$  emission reductions is insensitive to biases in the simulated  $\text{CH}_4$  distribution.

[17] Global distributions of  $\text{O}_3$  and its precursors in a different version of MOZART-2 were evaluated with available observations by Horowitz et al. [2003] who showed that the model generally captures the observed  $\text{O}_3$  seasonality, as well as horizontal and vertical gradients. On the regional scale, however, Murazaki and Hess [2006] previously showed a  $>20$  ppb mean bias in the MOZART-2

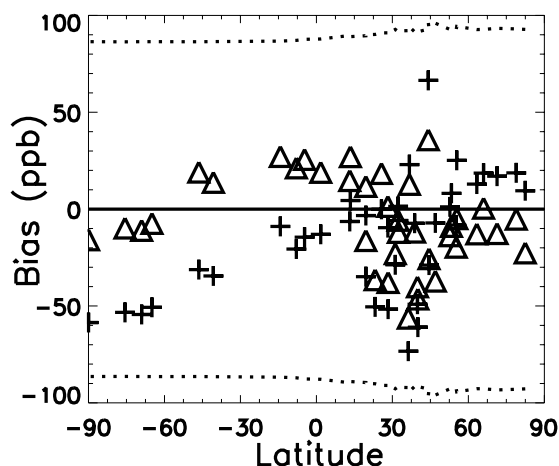


**Figure 3.** Annual mean bias (MOZART-2 model - NOAA observations) for  $\text{CH}_4$  abundance in dry surface air (ppb) in 2004, for year 15 of the BASE simulation (crosses) and the final year of a 5-year spin-up for the CLE simulations (triangles). The selected model years for both simulations use the 2004 NCEP meteorology. The model always falls within  $\pm 5\%$  of the observed values (dotted lines).

simulation of surface  $\text{O}_3$  as compared to the EPA AIRS monitoring sites over the eastern United States in summer. Our updated treatment of isoprene nitrates decreases simulated July afternoon surface  $\text{O}_3$  concentrations by 4–12 ppb over the eastern United States [Fiore *et al.*, 2005]. We note that the surface  $\text{O}_3$  sensitivity to  $\text{CH}_4$  does not appear to be strongly influenced by the remaining bias as our results below are consistent with the sensitivity previously diagnosed by the GEOS-Chem model, which exhibits a smaller bias compared to U.S. surface  $\text{O}_3$  observations [Fiore *et al.*, 2002a, 2002b, 2005].

[18] Most pertinent to our study is the ability of the model to represent the global distribution of  $\text{NO}_x$ . Horowitz *et al.* [2003] showed that the model typically fell within the observed range of  $\text{NO}_x$  concentrations throughout most of the troposphere. The largest discrepancies in  $\text{NO}_x$  concentrations occurred in surface air near islands, where the model overestimates measurements of clean marine boundary layer air due to mixing of emissions throughout the coarse-resolution grid cell [Horowitz *et al.*, 2003]. When we compare our CLE and BASE  $\text{NO}_x$  simulations for the meteorological year 2004 with the Horowitz *et al.* [2003] simulation, we find that the  $\text{NO}_x$  distributions are similar in most regions of the globe (not shown). The largest difference is found in the upper troposphere (beginning about 5–7 km), mainly in the tropical Pacific (e.g., over Christmas Island, Tahiti, Guam, the Philippine Sea) and in the southern Atlantic, where  $\text{NO}_x$  concentrations in our simulations are often lower than those by Horowitz *et al.* [2003] (and the observations) by a factor of two or more. This result likely reflects differences in the lightning  $\text{NO}_x$  distribution which is driven by the NCEP reanalysis in our simulations but by the NCAR MACCM3 meteorology by Horowitz *et al.* [2003]. In the ACCENT Photocomp Experiment 2, MOZART-2  $\text{NO}_2$  columns (in a simulation using year 2000 CLE emissions and  $\text{CH}_4$  concentrations set to

1760 ppb) were consistently 10–30% higher than the model ensemble mean [van Noije *et al.*, 2006]. The comparison with  $\text{NO}_2$  columns retrieved from the GOME instrument using three different methods varied widely, however, with MOZART-2 falling below the retrieved range in the Eastern U.S. (–3%), Eastern China (–15%) and South Africa (–48%); within the range in Europe and Northern Africa, and exceeding the range in Central Africa (+7%), South America (+39%), and Southeast Asia (+6%) [van Noije *et al.*, 2006].

## 2.5. Distribution of $\text{CH}_4$ Loss and $\text{O}_3$ Production in the BASE Simulation

[19] We examine the latitudinal and vertical distributions of  $\text{CH}_4$  and tropospheric  $\text{O}_3$  production in the BASE simulation, focusing here on the final year of the 30-year simulation. The strong temperature dependence of the  $\text{CH}_4$ -OH reaction largely restricts  $\text{CH}_4$  oxidation to the lower troposphere. Following the approach recommended by Lawrence *et al.* [2001], we find that 57% and 90% of the  $\text{CH}_4$  loss by reaction with OH occurs below 750 and 500 hPa, respectively (Table 3). This estimate is somewhat higher than previous work estimating that  $\text{CH}_4$  oxidation below 500 hPa accounts for  $\sim 80\%$  of the  $\text{CH}_4$  loss [Spivakovsky *et al.*, 2000; Lawrence *et al.*, 2001]. While it is possible that OH in MOZART-2 may be larger in the lower troposphere than in previous modeling studies, the  $\text{CH}_4$  lifetime against tropospheric OH is 10.3 years, within the range of other models (8.2–11.7 years based on Stevenson *et al.* [2006]). Most of the  $\text{CH}_4$  loss (75%) occurs in the tropics, consistent with the estimate by Spivakovsky *et al.* [2000] of 78% of  $\text{CH}_4$  loss between  $32^\circ\text{S}$  and  $32^\circ\text{N}$ . Table 3 also shows a hemispheric asymmetry, with nearly twice as much  $\text{CH}_4$  loss occurring north of  $30^\circ\text{N}$  than south of  $30^\circ\text{S}$ , and 20% more loss in the northern tropics than in the southern tropics. Since the  $\text{CH}_4$  burden is evenly distributed (<4% difference between the hemispheres), the asymmetry in the  $\text{CH}_4$  chemical loss reflects the OH distribution (Figure 4a), which in turn is governed by the larger  $\text{NO}_x$  emissions and resulting  $\text{NO}_x$  abundances in the northern hemisphere (Figure 4b). Ozone production in the model is also larger in the northern hemisphere, where shorter-lived anthropogenic  $\text{O}_3$  precursors are most abundant (e.g.,  $\text{NO}_x$  in Figure 4b), contributing  $\sim 60\%$  to the total global production, consistent with the estimate from Horowitz *et al.* [2003]. Our BASE simulation predicts a

**Table 3.** Spatial Distribution of  $\text{CH}_4$  Loss by Reaction With OH (BASE Simulation) and Change in Gross Tropospheric  $\text{O}_3$  Production (RGLOB-BASE Simulations)

	90–30S	30–0S	0–30N	30–90N	Total
<i>Methane loss by reaction with OH (%)</i>					
500–250 hPa	1.2	3.4	4.0	1.8	10.4
750–500 hPa	3.2	11.3	13.1	5.3	32.9
Surface–750 hPa	4.4	18.9	23.6	9.8	56.7
Total	8.8	33.6	40.7	16.9	100
<i>Change in gross ozone production (<math>\text{Tg a}^{-1}</math>)</i>					
500–250 hPa	–5.5	–11.5	–14.3	–8.4	–39.7
750–500 hPa	–5.8	–23.1	–26.3	–11.3	–66.5
Surface–750 hPa	–7	–23.5	–30.5	–23	–84
Total	–18.3	–58.1	–71.1	–42.7	–190.2

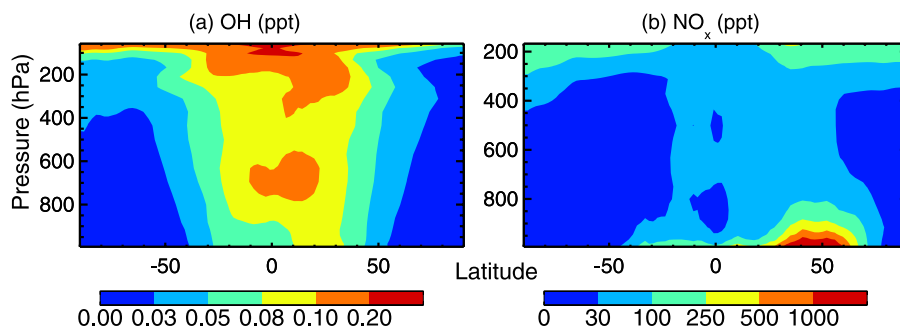


**Figure 4.** Zonal annual mean distributions of (a) OH and (b) NO<sub>x</sub> (ppt) in the BASE simulation in year 30.

slightly larger contribution from lower tropospheric O<sub>3</sub> production than by Horowitz *et al.* [2003] (51% versus 46%).

### 3. Linearity of Global Annual Mean O<sub>3</sub> Response to CH<sub>4</sub> Controls

[20] Figure 5 shows that the decreases in tropospheric CH<sub>4</sub> and O<sub>3</sub> from sustained CH<sub>4</sub> emission reductions (RGLOB-BASE) are approaching a steady state after 30 years of simulation. We use the final year of the simulations to diagnose the model “feedback factor”, the ratio of the perturbation lifetime ( $PT$ ; the decay time for a perturbation such as a pulse of CH<sub>4</sub> emissions) to the total atmospheric lifetime ( $LT = B/L_{CH_4}$ ):  $PT/LT = 1/(1 - s)$  where  $B$  is the total atmospheric CH<sub>4</sub> burden,  $L_{CH_4}$  is the total atmospheric CH<sub>4</sub> loss, and  $s = \delta \ln LT / \delta \ln B$  [Prather *et al.*, 2001]. We use the difference in lifetimes and burdens between the RGLOB and BASE simulations to calculate  $s = 0.23$ , corresponding to  $PT/LT = 1.30$ , somewhat smaller than the model range of 1.33–1.45 reported by Prather *et al.* [2001]. In the BASE simulation,  $LT = 8.7$  years, equal to

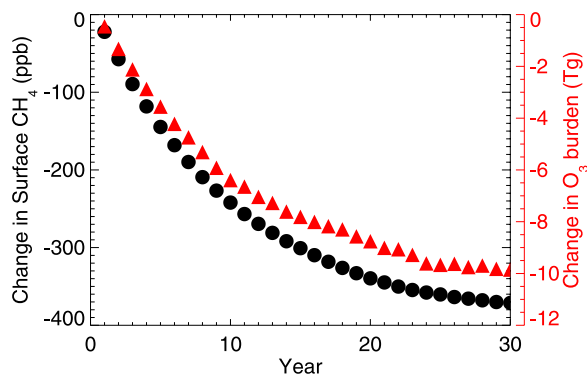


**Figure 5.** Annual mean change in surface CH<sub>4</sub> abundances (black circles; left axis) and in the tropospheric O<sub>3</sub> burden (red triangles; right axis), resulting from a 97 Tg a<sup>-1</sup> decrease in global anthropogenic CH<sub>4</sub> emissions relative to values in the same year of the BASE simulation (RGLOB-BASE) to remove the interannual variability due to meteorology. The 150 ppb O<sub>3</sub> chemical tropopause in the first year of the BASE simulation is used to calculate the tropospheric O<sub>3</sub> burden. In the first year of the BASE simulation, the total tropospheric O<sub>3</sub> burden is 300 Tg and the surface CH<sub>4</sub> abundance is 1720 ppb.

the mean of the range reported for current CTMs ( $8.7 \pm 1.3$  years) [Stevenson *et al.*, 2006]. We thus obtain a CH<sub>4</sub> perturbation time of 11.3 years and estimate that the model results in year 30 capture 93% ( $1 - e^{-30/11.3}$ ) of the steady state change, ultimately yielding a 23% steady state decrease in atmospheric CH<sub>4</sub> (1090 Tg CH<sub>4</sub> or 400 ppb surface mixing ratio) from the 18% decrease in total CH<sub>4</sub> emissions in RGLOB.

[21] We scale the tropospheric O<sub>3</sub> burden and surface O<sub>3</sub> responses (RGLOB-BASE) in year 30 to obtain ultimate steady state decreases of 10.3 Tg tropospheric O<sub>3</sub> (blue filled circle in Figure 1) and 1.0 ppb surface O<sub>3</sub> (global annual mean). The sensitivity of 0.11 Tg O<sub>3</sub> (or 11 ppt surface O<sub>3</sub>) decrease per Tg CH<sub>4</sub> a<sup>-1</sup> emission reduction diagnosed from these simulations is slightly lower than the 0.12–0.16 Tg O<sub>3</sub> range of the prior work displayed in Figure 1. In particular, the results of Shindell *et al.* [2005] (green squares in Figure 1) yield a larger sensitivity of  $\sim 0.16$  Tg O<sub>3</sub> per Tg CH<sub>4</sub> a<sup>-1</sup> emission.

[22] Annual mean results from the transient future scenarios (section 2.2) are shown in Figure 2. With the more aggressive controls in scenarios B and C, CH<sub>4</sub> concentrations decrease by 2030 to levels last observed in the 1990s and 1980s, respectively (Figure 2b). The tropospheric O<sub>3</sub> burden increases from 2005 to 2030 under all scenarios, by 17.0, 12.3, 7.7, and 2.8 Tg for scenarios CLE, A, B, and C, respectively (Figure 2c), reflecting the 19% growth in anthropogenic NO<sub>x</sub> emissions. The global annual mean 8-h daily maximum (MDA8) surface O<sub>3</sub> increases by 1.8 ppb in the baseline CLE scenario. The CH<sub>4</sub> control scenarios counteract some of this increase in surface O<sub>3</sub>, with the most aggressive CH<sub>4</sub> controls (scenario C) almost entirely offsetting this increase (total change of +0.2 ppb from 2005 to 2030; Figure 2d). Figures 2c and 2d illustrate the effect of interannual variability in meteorology on tropospheric O<sub>3</sub>, as evidenced by the repeating 5-year cycle superimposed upon the longer-term trend. This variability likely reflects year-to-year variations in lightning NO<sub>x</sub> emissions (which vary from 3.1–3.4 Tg N a<sup>-1</sup>) and/or exchange with the stratosphere (varies from 850–880 Tg a<sup>-1</sup>), both of which correlate strongly with annual mean tropospheric O<sub>3</sub> burdens in the BASE simulation with 1990–2004 meteorology ( $r^2 = 0.80$  and 0.92, respectively, for the first 15 year period).

[23] Although not at steady state, the results in Figure 2 scale approximately linearly to the emission changes, despite differences in the trajectory shapes of the emission controls over the 25 years. By comparing results for 2030 in

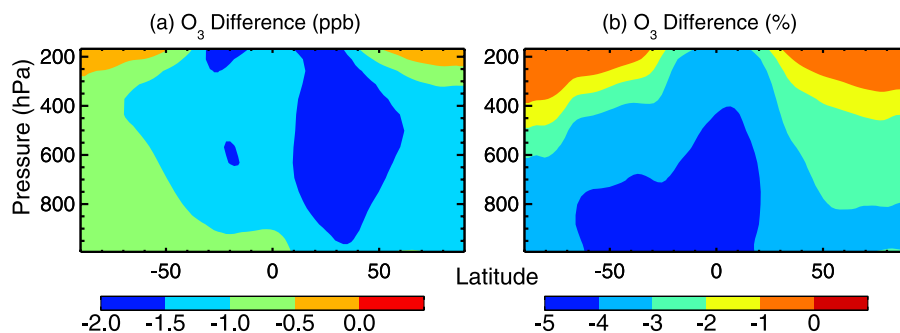


**Figure 6.** (a) Absolute and (b) percentage change in zonal annual mean  $O_3$  in year 30 due to a sustained  $97 \text{ Tg a}^{-1}$  reduction in global anthropogenic  $CH_4$  emissions (RGLOB-BASE).

scenarios A, B, and C with those from the baseline CLE simulation, we obtain a range of 0.06 (scenario A) to 0.08 (scenario C)  $\text{Tg } O_3$  decrease per  $\text{Tg } CH_4 \text{ a}^{-1}$  reduced. These values are lower than that from the RGLOB simulation since the CLE, A, B, and C simulations have not yet reached a steady state. The larger sensitivity implied by scenario C reflects the deeper  $CH_4$  reductions that are imposed earlier in this emission control trajectory (Figure 2a), allowing for a relatively larger  $O_3$  burden change to be realized by 2030. In an attempt to remove the influence of the shapes of the trajectories in Figure 2a on the results, we assume that the  $PT$  of 11.3 years diagnosed from RGLOB-BASE applies for the future scenarios (it may in fact differ since a different base emission inventory is used, which will influence OH). We then define an “effective  $CH_4$  emission control” in the year 2030 ( $\Delta E_{\text{eff-2030}}$ ) to represent the change in  $CH_4$  emissions that would produce a steady state response equal to the transient response in 2030 in each of our simulations (which are not at steady state). The  $\Delta E_{\text{eff-2030}}$  is calculated as the sum of the emission controls applied in each year from 2005 to 2030, weighted by the fraction of the steady state response that should be realized by 2030. In this manner, we estimate that  $\Delta E_{\text{eff-2030}}$  is  $-35$ ,  $-76$ , and  $-117 \text{ Tg } CH_4 \text{ a}^{-1}$  for scenarios A, B, and C, respectively, corresponding to a realization of 47%, 61%, and 65% of the total  $CH_4$  emission reductions by 2030. Using the  $\Delta E_{\text{eff-2030}}$ , we estimate revised sensitivities of 0.14, 0.12, and 0.12  $\text{Tg } O_3$  decrease per  $\text{Tg } CH_4 \text{ a}^{-1}$  “effective” emission reductions, in good agreement with the 0.12–0.16 range of the published results displayed in Figure 1, but slightly higher than the sensitivities obtained above from RGLOB-BASE. Finally, we use these sensitivities to obtain steady state changes in the  $O_3$  burden of 10.1, 15.3, and 21.8  $\text{Tg}$  for constant emissions at 2030 levels in scenarios A, B, and C, which we show in Figure 1. An alternative approach to diagnose  $\Delta E_{\text{eff-2030}}$  is to consider the change in the  $CH_4$  loss rate between the perturbation and baseline scenarios. With this approach, we estimate  $\Delta E_{\text{eff-2030}}$  of  $-44$ ,  $-86$ , and  $-130 \text{ Tg } CH_4 \text{ a}^{-1}$  for A, B, and C, respectively, which translate to sensitivities of 0.11  $\text{Tg } O_3$  decrease per  $\text{Tg } CH_4 \text{ a}^{-1}$  reduced, equivalent to that in RGLOB-BASE, and within 11–26% of the results obtained via the former approach.

[24] We next estimate the total contribution of anthropogenic  $CH_4$  emissions to tropospheric and surface  $O_3$  by comparing our  $CH_4$ -700 and CLE baseline simulations in 2030. The  $CH_4$  loss by tropospheric OH in the  $CH_4$ -700 simulation is  $235 \text{ Tg } CH_4 \text{ a}^{-1}$ . Using the lifetimes from

Prather *et al.* [2001] for  $CH_4$  loss to the stratosphere (120 years) and to soils (160 years), we estimate the total  $CH_4$  loss (equal to the implied emissions) to be  $265 \text{ Tg } CH_4 \text{ a}^{-1}$ . The implied emissions are thus within 10% of the  $245 \text{ Tg } CH_4 \text{ a}^{-1}$  natural plus biomass burning emissions in the baseline scenario (Table 2), indicating that this simulation can be used to estimate the impacts of setting 2030 anthropogenic  $CH_4$  emissions to zero. We note that zero anthropogenic  $CH_4$  could not possibly be achieved by 2030 even if anthropogenic emissions were shut off instantly in 2005, since some anthropogenic  $CH_4$  would still remain in the 2030 atmosphere ( $\sim 11\%$  for a  $PT$  of 11.3 years). We find that anthropogenic  $CH_4$  contributes 40  $\text{Tg}$  to the tropospheric  $O_3$  burden and 4 ppb to global annual mean surface concentrations in 2030. For comparison with the other simulations in Figure 1, we calculate the  $\Delta E_{\text{eff-2030}}$  for the baseline CLE scenario ( $+63 \text{ Tg } CH_4 \text{ a}^{-1}$ ), to estimate the steady state increase of  $+26 \text{ Tg}$  in the  $O_3$  burden. Relative to the steady state CLE value, the  $CH_4$ -700 simulation yields a decrease of 49  $\text{Tg } O_3$  (included in Figure 1) or a sensitivity of 0.11  $\text{Tg}$  tropospheric  $O_3$  (11 ppt surface  $O_3$ ) per  $\text{Tg } CH_4 \text{ a}^{-1}$  effective emission change, consistent with that diagnosed above from RGLOB-BASE.

[25] The similarity in the steady state  $O_3$  response to  $CH_4$  in our simulations and in the published literature implies that the  $CH_4$  and  $O_3$  changes resulting from perturbations to  $CH_4$  emissions can be accurately approximated, even when other OH precursors are evolving, by scaling to the effective  $CH_4$  emission change relative to the baseline  $CH_4$  emission scenario. Multiple computationally expensive transient simulations should only be needed in situations where OH changes substantially, as would be expected if  $CH_4$  emissions doubled [Prather, 1996]. In most cases, one steady state simulation relative to the baseline scenario should be sufficient to determine the model sensitivity of  $O_3$  (and its spatial distribution; see section 4) to  $CH_4$ . For estimating changes in global annual mean  $O_3$ , results can be approximated to within  $\sim 30\%$  without using a model, given the range of 0.11–0.16  $\text{Tg } O_3$  burden or 11–15 ppt surface  $O_3$  per  $\text{Tg } CH_4 \text{ a}^{-1}$  change in  $CH_4$  emission diagnosed from our simulations and the prior modeling studies in Figure 1.

#### 4. Spatial Distribution of the $O_3$ Response to Changes in $CH_4$ Emissions

[26] When anthropogenic  $CH_4$  emissions are reduced (in the RGLOB versus BASE simulations), gross  $O_3$  produc-

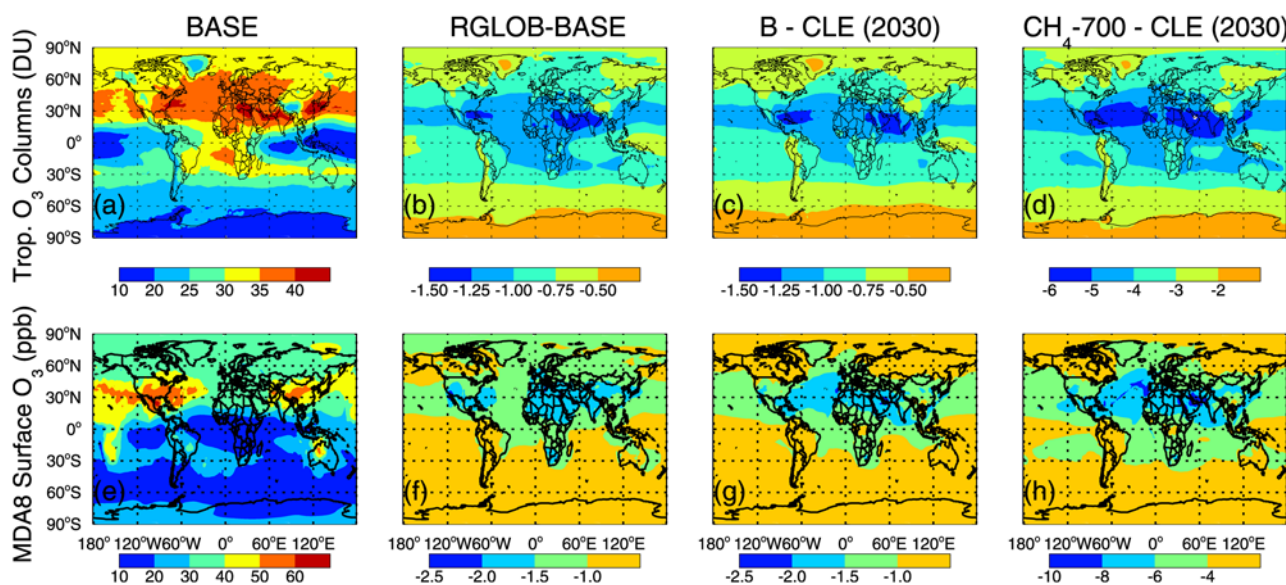


**Figure 7.** Annual mean tropospheric  $\text{O}_3$  columns (top row) and 8-h daily maximum (MDA8)  $\text{O}_3$  concentrations in surface air (bottom row) in the BASE simulation (a, e) and the change resulting from decreases in global anthropogenic  $\text{CH}_4$  emissions: RGLOB-BASE in year 30 (b, f), Scenario B - CLE in 2030 (c, g), and  $\text{CH}_4-700$  - CLE in 2030 (d, h). Note the different color scales for the  $\text{CH}_4-700$  results. Tropospheric  $\text{O}_3$  columns are calculated using the 150 ppb  $\text{O}_3$  chemical tropopause in BASE year 30 for the BASE and RGLOB simulations, and the CLE 2030 chemical tropopause for the CLE, B, and  $\text{CH}_4-700$  simulations.

tion and  $\text{O}_3$  concentrations decrease everywhere (Table 3 and Figure 6a), with the largest percentage changes occurring in the southern hemisphere (Figure 6b) where  $\text{CH}_4$  contributes to a larger fraction of the  $\text{O}_3$  production (since NMVOC abundances are lower than in the northern hemisphere). Annual mean  $\text{O}_3$  concentrations decrease by 0.5–2.0 ppb throughout the troposphere (Figure 6a), with the largest decreases centered around  $30^\circ\text{N}$  where OH and  $\text{NO}_x$  are enhanced in the lower troposphere compared to other latitudes (Figure 4). West and Fiore [2005] previously noted an enhanced response of surface  $\text{O}_3$  to  $\text{CH}_4$  decreases centered around  $30^\circ\text{N}$  and suggested that it reflects  $\text{O}_3$  production from  $\text{CH}_4$  in the free troposphere at these latitudes where  $\text{NO}_x$  is abundant, followed by downwelling of that air to the surface, a hypothesis that we examine further in section 5.

[27] We plot in Figure 7 the tropospheric  $\text{O}_3$  columns, relevant for climate forcing, as well as MDA8  $\text{O}_3$  concentrations in surface air, an indicator of air quality, in the BASE simulation. The highest annual mean tropospheric  $\text{O}_3$  columns and MDA8 surface  $\text{O}_3$  levels occur in the northern hemisphere over and downwind of continental regions where anthropogenic emissions of  $\text{O}_3$  precursors are largest (Figures 7a and 7e). Figure 7 also shows the  $\text{O}_3$  response to  $\text{CH}_4$  emission changes, which exhibits considerable spatial structure.

[28] Similar patterns of decreases in tropospheric  $\text{O}_3$  columns in response to  $\text{CH}_4$  controls occur in the RGLOB (Figure 7b) and scenario B (Figure 7c) simulations ( $r = 0.98$ ). While maximum  $\text{O}_3$  decreases are centered at  $30^\circ\text{N}$  (as in Figure 6a), large decreases in tropospheric  $\text{O}_3$  columns also extend southward into the tropical Atlantic ocean and Africa. Figures 7f and 7g show broadly similar patterns in the decreases of annual mean MDA8 surface  $\text{O}_3$  from  $\text{CH}_4$  controls, but the correlation is weaker than for the

tropospheric  $\text{O}_3$  columns ( $r = 0.88$ ). Figure 7f indicates that the largest benefits to air quality should occur over land, whereas the maximum decreases in surface  $\text{O}_3$  in Figures 7g and 7h are over the Gulf of Mexico, North Atlantic, and extend eastward across northern Africa and the Middle East into the Arabian Sea and Bay of Bengal. These discrepancies stem from differences in the  $\text{NO}_x$  emissions in the BASE and CLE inventories. For example, the model predicts a strong enhancement of  $\text{O}_3$  production (and a strong sensitivity to  $\text{CH}_4$ ) in  $\text{NO}_x$ -saturated ship track plumes in the CLE scenario, which does not occur in the sustained  $\text{CH}_4$  reduction scenarios where ship  $\text{NO}_x$  emissions were excluded (section 2.1). The dispersion of ship  $\text{NO}_x$  emissions into a coarse model grid box likely results in an artificially high  $\text{O}_3$  production efficiency [Kasibhatla et al., 2000; Liang and Jacobson, 2000] and we thus expect that the sensitivity of  $\text{O}_3$  to  $\text{CH}_4$  oxidation is overstated in the ship tracks in Figures 7g and 7h. Nevertheless, this result highlights that the  $\text{O}_3$  response to  $\text{CH}_4$  depends strongly on  $\text{NO}_x$ ; accurately representing the global  $\text{NO}_x$  distribution is thus important for simulating this sensitivity.

[29] The geographical patterns of the  $\text{O}_3$  response to  $\text{CH}_4$  controls are identical among the future  $\text{CH}_4$  control scenarios (A, B, C), implying that the  $\text{O}_3$  response is determined by the distribution of the shorter-lived species OH and  $\text{NO}_x$  which govern the  $\text{O}_3$  production from  $\text{CH}_4$  oxidation. As such, we focus in Figure 7 and thereafter on results from scenario B, noting that the magnitude of the  $\text{O}_3$  change scales linearly to the “effective  $\text{CH}_4$  emission controls” defined in section 3.

[30] Comparing the  $\text{O}_3$  response in scenario B with that in the  $\text{CH}_4-700$  simulation (third and fourth columns in Figure 7) illustrates that the  $\text{O}_3$  response exhibits an identical spatial pattern in a full transient  $\text{CH}_4$  simulation and in a simulation with  $\text{CH}_4$  set to a globally uniform, fixed value (spatial

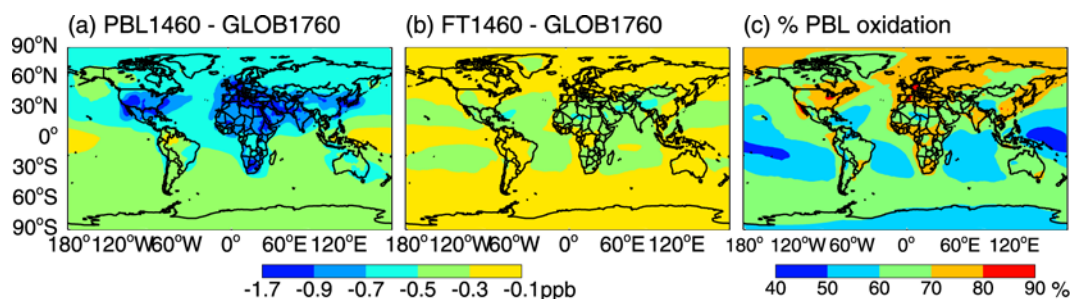


**Figure 8.** Change in annual mean MDA8 surface  $O_3$  (ppb) from reducing  $CH_4$  concentrations by 300 ppb (a) within the boundary layer (below 724 hPa) and (b) within the free troposphere, as diagnosed from steady state simulations (PBL1460-GLOB1760) and (FT1460-GLOB1760), respectively (Table 1). (c) Percentage contribution from  $CH_4$  oxidation within the planetary boundary layer to the total surface  $O_3$  change from  $CH_4$  reductions.

correlation of  $r = 1.0$  between Figures 7c and 7d, and between Figures 7g and 7h). This result indicates that the  $O_3$  response is insensitive to biases in the simulated  $CH_4$  distribution. Furthermore, the linearity of the  $O_3$  response to  $CH_4$  (Figure 1 and section 3) implies that the spatial pattern can be scaled to different magnitudes of  $CH_4$  controls.

[31] Finally, we examine the extent to which the spatial pattern of the surface  $O_3$  response varies with changes in meteorology in the final 15 years of our sustained  $CH_4$  reduction simulations (RGLOB-BASE). The interannual variability is  $<5\%$  in most world regions, except for in the tropics, on the west coast of central South America, and off the southwestern coast of United States where it is 10–20% (not shown). We conclude that the spatial patterns in Figure 7 are fairly robust to fluctuations in present-day meteorology.

## 5. Surface $O_3$ Contribution from $CH_4$ Oxidation in the Free Troposphere Versus Boundary Layer

[32] Surface  $O_3$  is influenced by  $CH_4$  oxidation both within the boundary layer and in the free troposphere (followed by subsidence of this air to the surface). With our steady state simulations (section 2.3), we separate the contributions to surface  $O_3$  from  $CH_4$  oxidation in these two regions. We focus our analysis on the PBL1460 and FT1460 simulations relative to GLOB1760 since we find our results to be linear; the  $O_3$  response to reductions of  $CH_4$  throughout the atmosphere (GLOB1460-GLOB1760) are virtually identical to the sum of the  $O_3$  changes from reducing  $CH_4$  in the boundary layer (PBL1460-GLOB1760) and from reducing  $CH_4$  in the free troposphere (FT1460-GLOB1760).

[33] At nearly all surface locations, oxidation of  $CH_4$  in the boundary layer contributes more than 50% of the change in annual mean MDA8  $O_3$  resulting from  $CH_4$  controls (Figure 8), with a global mean contribution of 64%. The 300 ppb decrease in boundary layer  $CH_4$  concentrations decreases MDA8  $O_3$  in surface air by up to 1 ppb  $O_3$  in the  $NO_x$ -rich regions of the northern midlatitudes and in southern Africa (Figure 8a). Surface  $O_3$  is also decreased by the reduction in  $CH_4$  oxidation in the free troposphere near the downwelling branches of the Hadley cell, at roughly  $30^\circ N$  and  $30^\circ S$ , particularly over the Sahara region of North Africa, the Middle East, and the Caribbean Sea where the 300 ppb decrease in free tropospheric  $CH_4$  concentrations lowers surface  $O_3$  by  $\sim 0.5$  ppb (Figure 8b).

[34] As a case study, we plot the composite maximum MDA8  $O_3$  decrease over the United States resulting from a 300 ppb decrease in  $CH_4$  in the planetary boundary layer (below 724 hPa; PBL1460-GLOB1760) in Figure 9. Southern California and the New York-New Jersey region in the northeastern United States exhibit a larger peak  $O_3$  decrease ( $>2-3$  ppb) from the  $CH_4$  reduction than the rest of the country. In these  $NO_x$ -saturated regions,  $CH_4$  oxidation within the planetary boundary layer accounts for 70–80% of the total  $O_3$  decrease from  $CH_4$  reductions (Figure 8c). We conclude that the surface  $O_3$  response to  $CH_4$  is strongly enhanced in locations with  $NO_x$ -saturated chemistry, and weakly enhanced in regions of downwelling air.

[35] The question arises as to whether our coarse resolution global model accurately represents the response of  $O_3$  to  $CH_4$  at the urban scale. Higher-resolution model calculations of  $O_3$  production in urban airsheds support the conclusion that  $O_3$  production in polluted urban areas is sensitive to  $CH_4$ . For example, it has been estimated that despite its low reactivity,  $CH_4$  oxidation contributes approximately 10–20% of the  $O_3$  formed downwind of London in the urban plume [Hough and Derwent, 1987; Derwent *et al.*, 1991]. Martien and Harley [2006] used adjoint methods to identify a strong VOC-sensitivity in and downwind of core urban areas. The consistency of our global model results with the conclusions from these studies implies that the global model is useful in assessing the qualitative  $O_3$

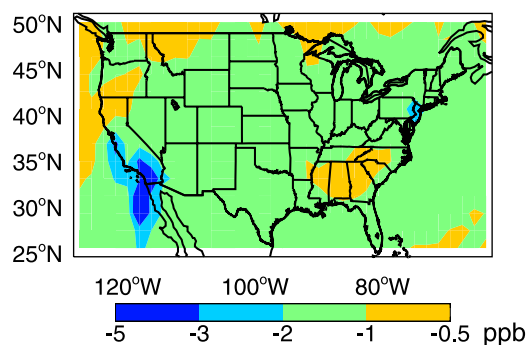


**Figure 9.** Composite maximum change in U.S. MDA8 surface  $O_3$  occurring in each model grid cell on any day between 1 June to 31 August from reducing  $CH_4$  concentrations by 300 ppb within the boundary layer (below 724 hPa; PBL1460-GLOB1760).

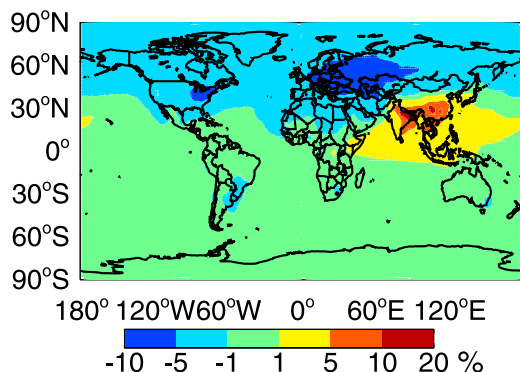


**Figure 10.** The percentage difference of the change in annual mean MDA8 surface  $O_3$  in simulation year 11 in the RASIA and RGLOB simulations, calculated as  $100 \cdot (\text{RASIA} - \text{RGLOB}) / (\text{RGLOB} - \text{BASE})$ .

response to  $CH_4$  in urban areas, although the accuracy of the results for a particular urban core will depend upon the model representation of the VOC- $NO_x$  sensitivity.

## 6. Sensitivity of Tropospheric $O_3$ to the Location of $CH_4$ Emissions

[36] Given the long lifetime of  $CH_4$ , the  $O_3$  produced from  $CH_4$  oxidation is expected to be independent of the location of the  $CH_4$  emissions. Instead, the spatial pattern of the  $O_3$  from  $CH_4$  oxidation should be controlled by the distributions of OH and  $NO_x$ , which have much shorter lifetimes and affect both the location of the  $CH_4$  oxidation and the amount of  $O_3$  produced per  $CH_4$  molecule oxidized. We directly test this assumption by comparing the results from the RASIA simulation, in which Asian anthropogenic  $CH_4$  emissions are set to zero, with those from the RGLOB simulation, in which an equivalent  $CH_4$  emission reduction was distributed globally.

[37] Figure 10 compares the MDA8 surface  $O_3$  in RASIA and RGLOB simulations in year 11 (note that The RASIA simulation was stopped after 11 years since there was little difference in the  $O_3$  response from that in RGLOB). Except for the immediate source region over Asia, there is  $<10\%$  difference in other northern hemispheric source regions,  $<5\%$  difference over the rest of the northern hemisphere, and  $<1\%$  difference in the southern hemisphere. Annual mean tropospheric  $O_3$  columns in year 11 are even more similar between the simulations ( $<0.5\%$  differences; not shown). These results imply that control options could be targeted starting with the least cost reductions available anywhere in the world since the global air quality and climate benefits of  $CH_4$  controls do not depend strongly upon the location of the emission reductions.

## 7. Regional Air Quality

[38] We first investigate the seasonality of the regional surface  $O_3$  response to  $CH_4$  using the simulations with sustained  $CH_4$  reductions (RGLOB-BASE; Figure 11). Both Europe and South Asia show some seasonal variation (0.8 and 0.5 ppb amplitude, respectively) whereas there is little seasonality over the United States, East Asia and Africa.

These results are consistent with the findings from a multi-model intercomparison of the surface  $O_3$  response to a 20% decrease in global  $CH_4$  mixing ratios, although the regional definitions in that study are not identical [*Task Force on Hemispheric Transport of Air Pollution (TF HTAP)*, 2007]. The enhanced response over Europe in summertime and over South Asia in April may reflect a more  $NO_x$ -saturated  $O_3$  formation regime than during the peak  $O_3$  seasons in the United States and Africa, where biogenic VOC are more abundant.

[39] Next, we examine the percentage of model grid box-days where MDA8  $O_3 \geq 70$  ppb in surface air (a metric for polluted conditions) by season for the selected world regions in the future scenarios. Figure 12 shows that air quality degrades substantially under the baseline CLE scenario from 2005 to 2030 in South Asia, where large growth in emissions ( $+58\%$  for  $NO_x$ ) from the transport and power generation sectors is projected [*Dentener et al.*, 2005]. From 2005 to 2030, the percentage of model grid cell-days with MDA8  $O_3 \geq 70$  ppb increases by 4%, 1%, and 2% in the United States, Europe, and Africa, respectively, during summer, the season in which high- $O_3$  events peak for those regions (Figure 12). Peak incidences occur in spring in the Asian regions, with increases of 4% (for East Asia) and 14% (for South Asia) in the percentage of model grid cell-days with MDA8  $O_3 \geq 70$  ppb from 2005 to 2030. These findings are consistent with prior modeling studies in which the CLE scenario produced surface  $O_3$  increases of  $\sim 10$  ppb over the Indian subcontinent from 2000 to 2030, and of  $\sim 2$  ppb globally, with little change over some regions of North America, Europe and Asia [*Dentener et al.*, 2006b; *Stevenson et al.*, 2006].

[40] We evaluate here the ability of the global model to represent the threshold statistic presented in Figure 12, and determine whether those results can be extended to other thresholds. A similar statistic was previously used by *Fiore et al.* [2002a] who found that a global model was able to

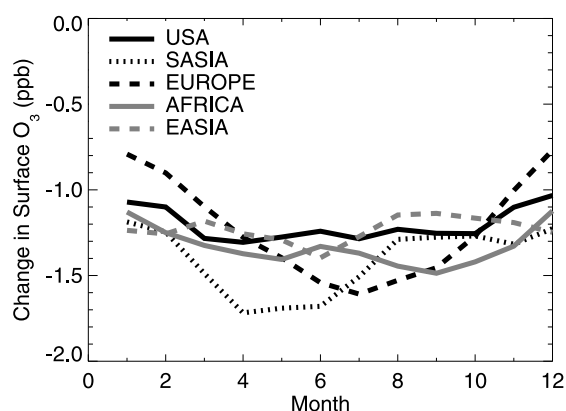


**Figure 11.** Monthly mean change in surface  $O_3$  over land boxes ( $\geq 50\%$  land) in selected regions, resulting from a sustained  $97 \text{ Tg a}^{-1}$  reduction in global anthropogenic  $CH_4$  emissions after 30 years of simulation (RGLOB-BASE). The regions are defined as: USA ( $62.5\text{--}127.5^\circ\text{W}$ ;  $24\text{--}52^\circ\text{N}$ ; solid black), EUROPE ( $10^\circ\text{W}\text{--}50^\circ\text{E}$ ;  $35\text{--}70^\circ\text{N}$ ; dashed black), SOUTH ASIA ( $50\text{--}100^\circ\text{E}$ ;  $5\text{--}35^\circ\text{N}$ ; dotted black), EAST ASIA ( $100\text{--}150^\circ\text{E}$ ;  $25\text{--}50^\circ\text{N}$ ; dashed grey), AFRICA ( $20^\circ\text{W}\text{--}50^\circ\text{E}$ ;  $35^\circ\text{S}\text{--}35^\circ\text{N}$ ; solid grey).

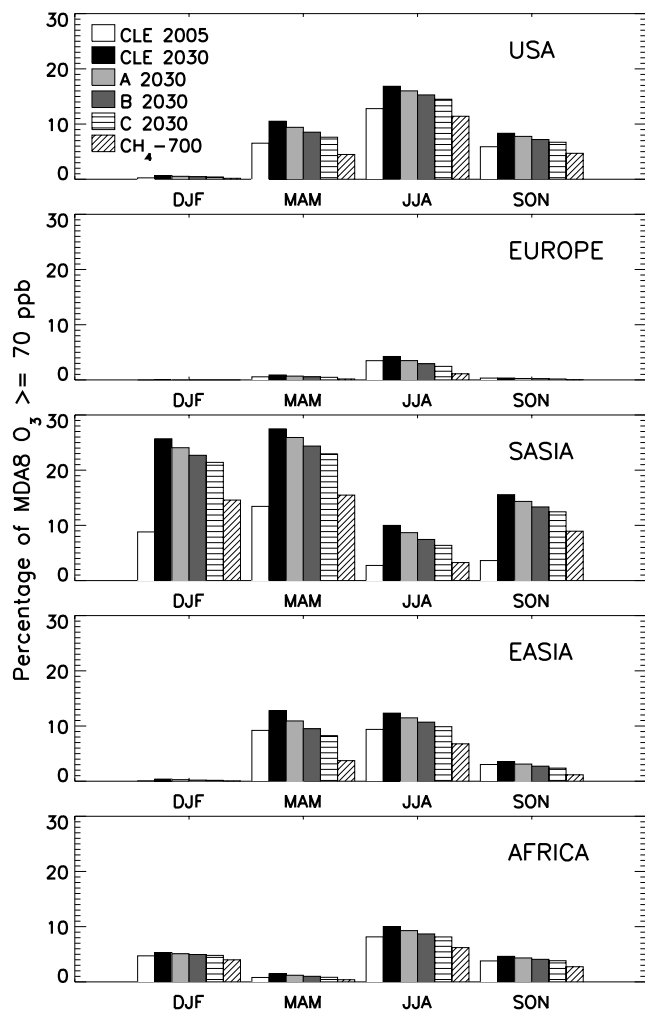


**Figure 12.** Percentage of model grid-cell days with MDA8 surface O<sub>3</sub> concentrations  $\geq 70$  ppb by season and region for the future scenarios described in section 2.2: CLE 2005 (white); CLE 2030 (black); A (light grey), B (dark grey), and C (horizontal stripes) in 2030; and CH<sub>4</sub>-700 (angled stripes). The regions are defined in the caption to Figure 11.

simulate adequately the percentage of total grid box-days above 70 ppb in the United States during the summer of 1995 (observed values of 5%, 15% and 36% for thresholds of 80, 70, and 60 ppb and simulated values of 1%, 10%, and 37%). In our CLE simulation for 2005, we find that 5%, 13% and 26% of grid box-days over the United States in summer exceed 80, 70, and 60 ppb thresholds, respectively. We further find that the changes due to CH<sub>4</sub> emission controls are relatively insensitive to the chosen threshold, such that in 2030, scenario A yields a  $\sim 5\%$  decrease in the incidence of grid box-days above 60, 70, and 80 ppb relative to the CLE scenario. For scenarios B, C, and CH<sub>4</sub>-700, the corresponding percentage changes are  $\sim 10\%$ ,  $\sim 15\%$ , and  $\sim 35\%$ . Below, we focus on results for the 70 ppb threshold.

[41] All of our CH<sub>4</sub> reduction scenarios decrease the percentage of model grid cell-days with MDA8 O<sub>3</sub>  $\geq 70$  ppb in 2030, by up to 3% (Europe) to 12% (South Asia) when all anthropogenic CH<sub>4</sub> is removed (Figure 12). The cost-

effective CH<sub>4</sub> reductions in scenario B yield percentage decreases of 1%, 1%, and 2% in Africa, Europe, and the United States in summer, and of 3% in both Asian regions in spring compared to CLE. For all regions, the largest decreases in the percentage of high-O<sub>3</sub> events occurs in the same season as the peak number of model grid cell-days with MDA8 O<sub>3</sub>  $\geq 70$  ppb, except for the United States where the decrease is slightly larger in spring.

[42] During summer in Europe and fall in East Asia, aggressive CH<sub>4</sub> controls (scenarios B and C) would decrease high-O<sub>3</sub> events to below 2005 levels. For the United States and Africa, only the CH<sub>4</sub>-700 simulation reduces high-O<sub>3</sub> events below the 2005 levels. The dramatic growth of O<sub>3</sub> precursor emissions over South Asia leads to additional model grid-cell days where MDA8 O<sub>3</sub>  $\geq 70$  ppb, even with the drastic reduction of CH<sub>4</sub> to pre-industrial levels.

[43] In Figure 13, we assess the potential for CH<sub>4</sub> controls to reduce MDA8 O<sub>3</sub> in surface air under background, average, and highly polluted conditions. We focus on the high-O<sub>3</sub> season for each region, when the incidence of grid-square days  $\geq 70$  ppb is maximum in the year 2030, and plot the distribution of the change in MDA8 surface O<sub>3</sub> in response to the CH<sub>4</sub> controls in scenario B (B-CLE), as a function of the MDA8 O<sub>3</sub> values in the baseline CLE simulation for the year 2030. Within the United States, results are shown for the four quadrants in order to illustrate differences that can occur within large continental-scale regions.

[44] The median O<sub>3</sub> decrease tends to grow linearly to a maximum of  $\sim 2$  ppb at CLE 2030 MDA8 O<sub>3</sub> concentrations of 60–90 ppb (Figure 13). In contrast, the median response in the western U.S. quadrants increases linearly over the entire O<sub>3</sub> distribution, with days when total O<sub>3</sub>  $> 90$  ppb nearly always associated with decreases of  $> 1$  ppb and  $> 2.5$  ppb for the northwestern and southwestern quadrants, respectively; these conditions are typically associated with boundary layer stagnation and the strong O<sub>3</sub> response reflects the relatively high sensitivity to CH<sub>4</sub> oxidation in the polluted boundary layer in southern California (Figures 8 and 9). In Figure 13, O<sub>3</sub> also exhibits a strong sensitivity to CH<sub>4</sub> on the most polluted grid-cell days ( $> 90$  ppb) in Europe, East Asia, and Africa, often decreasing by  $> 1$  ppb under scenario B.

[45] The median response in the southeastern U.S. quadrant peaks at  $\sim 40$  ppb total O<sub>3</sub> and then weakens as total O<sub>3</sub> increases further. This feature reflects the meteorology in the southeastern U.S. in summer. The cleanest conditions are associated with inflow of marine air from the Gulf of Mexico; the stronger median sensitivity at 10–40 ppb total O<sub>3</sub> over the southeastern U.S. compared to the other U.S. regions in Figure 13, stems from the enhanced contribution of CH<sub>4</sub> oxidation in the free troposphere (followed by mixing into the boundary layer) over the Gulf of Mexico (Figure 8). The most polluted conditions are associated with stagnation events that suppress mixing between the free troposphere and boundary layer [Logan, 1989; Eder et al., 1993; Jacob et al., 1993]. Given that O<sub>3</sub> chemistry over the southeastern United States is NO<sub>x</sub>-sensitive due to abundant biogenic VOC emissions [Chameides et al., 1988], CH<sub>4</sub> contributes less to O<sub>3</sub> on the most polluted days than in the NO<sub>x</sub>-saturated regions of the western and northeastern United States.

[46] Peak decreases of  $\geq 4$  ppb (indicated by the lower extent of the vertical lines in Figure 13) occur near the

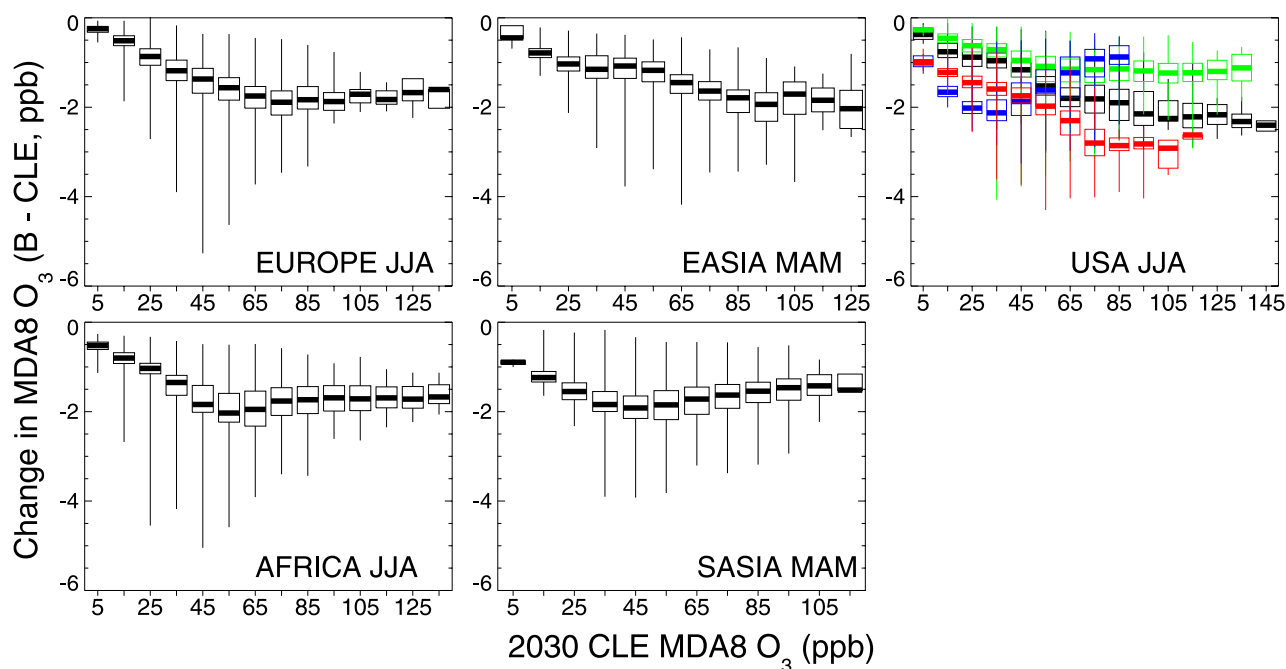


**Figure 13.** Change in MDA8 surface  $O_3$  concentrations in 2030 resulting from the  $CH_4$  controls in Scenario B (B-CLE), plotted against the MDA8  $O_3$  value in 2030 in the baseline CLE scenario, for each 10 ppb bin. The boxes enclose the 25th–75th percentiles, with the median denoted by the thick horizontal line. Vertical lines represent the full range of values for each bin. The distribution is constructed from the 92 daily values from each grid cell in the region for summer (Europe, Africa, USA) or spring (East Asia and South Asia). Region boundaries are given in the caption to Figure 11. The USA is subdivided into four quadrants at  $100^\circ W$  and  $35^\circ N$ : northeast (green), southeast (blue), southwest (red), and northwest (black).

center of the overall distribution, within the range of 40–60 ppb for Europe; 20–70 ppb for Africa; 40–70 ppb for East Asia, 30–60 ppb for South Asia, and 30–100 ppb in the United States. Emissions of  $NO_x$ , CO, and NMVOC emissions on foreign continents were previously shown to exert a maximum influence on U.S. surface  $O_3$  near the middle of the total  $O_3$  distribution, under conditions of strong mixing with the free troposphere [e.g., Fiore *et al.*, 2002b; Li *et al.*, 2002]. Similarly, the highest U.S. background  $O_3$  concentrations (estimated in simulations where North American anthropogenic emissions of  $NO_x$ , CO, and NMVOC were turned off but  $O_3$  generated from  $CH_4$  oxidation was included) were found at the center of the overall surface  $O_3$  distribution and attributed to  $O_3$  mixing down from the free troposphere [Fiore *et al.*, 2003]. The qualitative similarity of the results in Figure 13 to prior studies provides some confidence that our findings are robust to the model bias in surface  $O_3$  (section 2.4) although we cannot rule out some influence of the bias on the quantitative results, particularly at the high tail of the  $O_3$  distribution.

[47] We conclude that the scatter in the MDA8  $O_3$  changes in Figure 13 likely reflects differences in meteorology (mixing with the free troposphere versus local stagnation) as well as in chemistry (the local sensitivity of ozone production to  $CH_4$ ). The smaller sensitivity to  $CH_4$  at the low end of the total  $O_3$  distribution reflects cleaner air and does not necessarily imply a lack of mixing between the boundary layer and the free troposphere. The larger than average response in the upper tail of the total  $O_3$  distribution

over most regions typically occurs under stagnant conditions and is driven by the local  $NO_x$ -saturated chemistry.

## 8. Climate Forcing

[48] We estimate the radiative forcings from  $CH_4$  and  $O_3$  resulting from  $CH_4$  emission reductions as a proxy for the climate response. For  $CH_4$ , we evaluate the analytical expression recommended by Ramaswamy *et al.* [2001], using the calculated global mean  $CH_4$  concentrations to estimate the global mean adjusted forcing. Assuming a homogenous spatial distribution for  $CH_4$  has been shown to introduce an error much less than 1% in radiative forcing relative to a calculation using a  $CH_4$  distribution simulated by a CTM [Ramaswamy *et al.*, 2001]. The adjusted forcing from tropospheric  $O_3$  is calculated with the GFDL AM2 radiative transfer model [Freidenreich and Ramaswamy, 1999; Schwarzkopf and Ramaswamy, 1999; Geophysical Fluid Dynamics Laboratory (GFDL) Global Atmospheric Model Development Team (GAMDT), 2004], with stratospheric temperature adjustment following the approach of Naik *et al.* [2007]. We caution that the spatial pattern of the temperature response will not generally follow that of the radiative forcing [Levy *et al.*, 2008], and a full climate model simulation would be needed to estimate the temperature response to the forcings shown here.

[49] The global mean  $O_3$  radiative forcing under the CLE baseline scenario (2030–2005) is  $0.065 \text{ W m}^{-2}$ , near the multimodel mean in the CLE scenario from 2000 to 2030

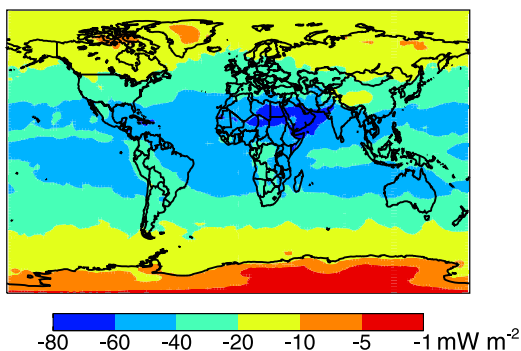


**Figure 14.** Adjusted radiative forcing from tropospheric  $O_3$  in scenario B relative to the CLE baseline, for the year 2030 ( $mW m^{-2}$ ).

( $0.063 \pm 0.015 W m^{-2}$ ) reported by *Stevenson et al.* [2006]. The strongest forcing occurs in the tropics, particularly over South Asia and the Middle East regions ( $0.15\text{--}0.21 W m^{-2}$ ) where the increases in tropospheric  $O_3$  columns are largest (not shown). All of the  $CH_4$  control scenarios yield a similar spatial pattern of decreases in  $O_3$  forcing, with the largest decreases occurring broadly in the tropics and over the Middle East and northern Africa (Figure 14). The larger forcings in the tropics as compared to the poles reflect the spatial pattern of the change in tropospheric  $O_3$  columns (Figure 7c) and the higher sensitivity of the forcing to the  $O_3$  column at these latitudes (forcing efficiencies of  $0.04\text{--}0.06$  versus a global mean of  $0.036 W m^{-2} DU^{-1}$ ). Table 4 shows the global mean forcing from both  $CH_4$  and  $O_3$  for each 2030 sensitivity simulation. Aggressive  $CH_4$  controls (scenarios B and C) would offset the positive net forcing from  $CH_4$  and  $O_3$  predicted to occur otherwise from 2005 to 2030 under the baseline CLE scenario. While the global mean forcing from  $CH_4$  and  $O_3$  roughly cancel in scenario B, we expect regional variations; for example, the positive forcing from  $O_3$  may exceed the negative forcing from  $CH_4$  in the tropics, with the opposite impact near the poles. Eliminating anthropogenic  $CH_4$  emissions would reduce global mean radiative forcing from  $CH_4$  and  $O_3$  by  $0.6 W m^{-2}$  relative to 2005 (by  $0.7 W m^{-2}$  relative to the CLE 2030 baseline).

## 9. Conclusions

[50] The potential to improve both climate and air quality by regulating  $CH_4$  emissions has sparked discussion of  $CH_4$  controls as a component of future air pollution policy [EMEP, 2005; TF HTAP, 2007]. Our analysis expands upon prior modeling studies [Fiore et al., 2002a; Dentener et al., 2005; West et al., 2006, 2008] to provide a basis for more fully assessing the monetary costs and benefits associated with managing global  $O_3$  pollution by controlling  $CH_4$  emissions [West et al., manuscript in preparation, 2007]. We employed two sets of full-chemistry multidecadal transient simulations in the MOZART-2 global CTM to characterize the response of  $CH_4$  and  $O_3$  to changes in  $CH_4$  emissions, and to estimate the  $O_3$  air quality and climate benefits that would result from  $CH_4$  controls. We further diagnosed the relative impact of  $CH_4$  oxidation in the free troposphere versus in the boundary layer on surface  $O_3$ , as

well as the anthropogenic  $CH_4$  contribution to tropospheric  $O_3$ , with a set of steady state simulations.

[51] Cost-effective future  $CH_4$  controls through 2030 (our scenario B;  $<\$315$  per ton  $CH_4$ ) would offset the projected positive climate forcing from  $CH_4$  and  $O_3$ , and reduce the incidence of high surface  $O_3$  events in all regions relative to the CLE baseline scenario; air quality would improve even relative to 2005 in Europe (summer and fall) and East Asia (fall). The mean  $O_3$  decrease from  $CH_4$  controls is often largest near the middle of the total  $O_3$  distribution (e.g.,  $\sim 40\text{--}70$  ppb total  $O_3$ ). Even during high- $O_3$  events,  $O_3$  often decreases by  $>1$  ppb in scenario B by 2030. Controlling  $CH_4$  emissions could thus help to achieve compliance with air quality standards, particularly in situations where high- $O_3$  events are frequently within a few ppb of a threshold concentration, as is often the case in the United States.

[52] Combining our results with estimates from the published literature, we find that global tropospheric  $O_3$  decreases approximately linearly with reductions in  $CH_4$  emissions:  $0.11\text{--}0.16 Tg$  tropospheric  $O_3$  or  $11\text{--}15 ppt$  surface  $O_3$  per  $Tg CH_4 a^{-1}$ . This sensitivity implies a total contribution from present-day anthropogenic  $CH_4$  emissions of  $\sim 50 Tg$  to the tropospheric  $O_3$  burden and  $\sim 5 ppb$  to surface  $O_3$ . The similarity of the global mean sensitivity of  $O_3$  to  $CH_4$  in our simulations and those from other models shown in Figure 1, and of the spatial pattern in our transient and steady state simulations (Figures 7c and 7g versus Figures 7d and 7h) indicates that the  $O_3$  response to  $CH_4$  is insensitive to biases in the simulated  $CH_4$  distribution and thus to errors in the spatial distribution of emissions. We further expect that the sensitivity of  $O_3$  to  $CH_4$  in MOZART-2 is fairly robust to the positive surface  $O_3$  bias versus observations over the eastern United States [Fiore et al., 2005; Murazaki and Hess, 2006], based on the consistency of our results with the other models in Figure 1, and of the results in Figures 12 and 13 with prior simulations with the GEOS-Chem model which has a much smaller bias compared to the observations [Fiore et al., 2002a, 2002b, 2005].

[53] We defined an “effective  $CH_4$  emission change” to facilitate comparisons between transient and steady state results. In the case of our future simulations, the effective  $CH_4$  emission change in 2030 ( $\Delta E_{\text{eff-2030}}$ ) is the sum of the emission controls applied in each year from 2005 to 2030, weighted by the fraction of the steady state response that should be realized by 2030. We showed that once the relationship between  $\Delta E_{\text{eff-2030}}$  and the resulting  $CH_4$  concentration is established for a baseline scenario (in

**Table 4.** Adjusted Radiative Forcing ( $W m^{-2}$ ) in 2030 Versus 2005 Due to Changes in Tropospheric  $CH_4$  and  $O_3$

Simulation	$CH_4^a$	$O_3^b$
CLE	0.099	0.065
A	0.033	0.048
B	$-0.029$	0.032
C	$-0.097$	0.014
$CH_4\text{-}700$	$-0.501$	$-0.080$

<sup>a</sup>Calculated with the analytic expression from *Ramaswamy et al.* [2001].

<sup>b</sup>Calculated in the GFDL AM2 radiative transfer model, including stratospheric adjustment following the approach of *Naik et al.* [2007]. The tropospheric  $O_3$  forcing is dominated by longwave radiation, with a 21–25% contribution from shortwave.

which emissions of NO<sub>x</sub> and other OH precursors are evolving), the CH<sub>4</sub> and O<sub>3</sub> changes that would result from perturbing CH<sub>4</sub> emissions by a different magnitude relative to that scenario can be accurately approximated, eliminating the need for multiple computationally expensive transient simulations (as long as the OH is relatively constant). In many cases, one steady state simulation relative to the baseline scenario should be sufficient to determine the model sensitivity of O<sub>3</sub> to CH<sub>4</sub>, including the spatial distribution of the O<sub>3</sub> response. For estimating changes in annual global mean O<sub>3</sub>, results can be approximated to within ~30% using the sensitivity estimated here, without needing additional model simulations.

[54] The decreases in surface O<sub>3</sub> and tropospheric O<sub>3</sub> columns (relevant for air quality and climate, respectively) arising from CH<sub>4</sub> emission control are largely independent of source location, with the exception of ~10–20% enhancements in source regions. Although the surface O<sub>3</sub> response to CH<sub>4</sub> emission reductions is relatively homogeneous across the globe compared with the response to controls on NO<sub>x</sub> emissions [West et al., 2008], the decreases in surface O<sub>3</sub> are not uniform, reflecting a combination of local meteorological and chemical conditions.

[55] We find in the model that global annual mean maximum daily 8-h (MDA8) surface O<sub>3</sub> is nearly twice as sensitive to CH<sub>4</sub> in the planetary boundary layer (below ~2.5 km) than to CH<sub>4</sub> in the free troposphere. The surface O<sub>3</sub> response to CH<sub>4</sub> is strongly enhanced in locations with NO<sub>x</sub>-saturated chemistry, including at the high tail of the O<sub>3</sub> distribution (e.g., in southern California). Weaker enhancements occur in regions where surface air mixes frequently with the free troposphere, either due to subsiding air masses (such as over northern Africa and the Middle East) or due to active convection (such as over the Caribbean Sea and Gulf Coast of the United States).

[56] Since the O<sub>3</sub> response to CH<sub>4</sub> depends strongly on NO<sub>x</sub>, we underscore the need for a better understanding of the global NO<sub>x</sub> distribution. A key policy implication from our study is that the efficacy of CH<sub>4</sub> emission reductions for addressing global air quality and climate goals is nearly independent of the location of the emissions. This result is particularly important given the rising cost of implementing additional controls on the traditional O<sub>3</sub> precursors in many nations where these emissions have already been regulated for decades. Accurate determination of CH<sub>4</sub> emissions by region and sector will nevertheless be critical for estimating the costs and technical feasibility of various options for CH<sub>4</sub> control, as well as for understanding the relative contributions from anthropogenic and natural CH<sub>4</sub> sources.

[57] **Acknowledgments.** We are grateful to F.J. Dentener for providing the baseline CLE and MFR emissions and J.S. Wang for providing the biogenic emissions, and to E. Baum, J. Chai, R.G. Derwent, H. Levy II, R. A. Harley, D. D. Parrish, D. Shindell, S. Sillman, and A. Zuber for insightful discussions. We acknowledge funding from Luce Foundation via Clean Air Task Force.

## References

- Brasseur, G. P., X. X. Tie, P. J. Rasch, and F. Lefèvre (1997), A three-dimensional simulation of the Antarctic ozone hole: Impact of anthropogenic chlorine on the lower stratosphere and upper troposphere, *J. Geophys. Res.*, *102*, 8909–8930.
- Carter, W. P. L., and R. Atkinson (1996), Development and evaluation of a detailed mechanism for the atmospheric reactions of isoprene and NO<sub>x</sub>, *Int. J. Chem. Kinet.*, *28*, 497–530.
- Chameides, W. L., R. W. Lindsay, J. Richardson, and C. S. Kiang (1988), The role of biogenic hydrocarbons in urban photochemical smog: Atlanta as a case study, *Science*, *241*, 1473–1475.
- Chen, X., D. Hulbert, and P. B. Shepson (1998), Measurement of the organic nitrate yield from OH reaction with isoprene, *J. Geophys. Res.*, *103*, 25,563–25,568.
- Chen, G., et al. (2005), An investigation of the chemistry of ship emission plumes during ITCT 2002, *J. Geophys. Res.*, *110*, D10S90, doi:10.1029/2004JD005236.
- Cofala, J., M. Amann, Z. Klimont, and W. Schöpp (2005), Scenarios of world anthropogenic emissions of SO<sub>2</sub>, NO<sub>x</sub>, and CO up to 2030, in *Internal Report of the Transboundary Air Pollution Programme*, p. 17, [http://www.iiasa.ac.at/rains/global\\_emiss/global\\_emiss.html](http://www.iiasa.ac.at/rains/global_emiss/global_emiss.html), International Institute for Applied Systems Analysis, Laxenburg, Austria.
- Crutzen, P. (1973), A discussion of the chemistry of some minor constituents in the stratosphere and troposphere, *Pure Appl. Geophys.*, *106–108*, 1385–1399.
- Denman, K. L., et al. (2007), Couplings Between Changes in the Climate System and Biogeochemistry, in *Climate Change 2007: The Physical Science Basis, Contribution of Working Group I to the Fourth Assessment Report of the Intergovernmental Panel on Climate Change*, edited by S. Solomon et al., Cambridge University Press, Cambridge, United Kingdom and New York, NY, USA.
- Dentener, F., D. Stevenson, J. Cofala, R. Mechler, M. Amann, P. Bergamaschi, F. Raes, and R. Derwent (2005), The impact of air pollutant and methane emission controls on tropospheric ozone and radiative forcing: CTM calculations for the period 1990–2030, *Atmos. Chem. Phys.*, *5*, 1731–1755.
- Dentener, F., et al. (2006a), Nitrogen and sulfur deposition on regional and global scales: A multi-model evaluation, *Global Biogeochem. Cycles*, *20*, GB4003, doi:10.1029/2005GB002672.
- Dentener, F., et al. (2006b), The global atmospheric environment for the next generation, *Environ. Sci. Technol.*, *40*, 3586–3594.
- Derwent, R. G., G. Grennfelt, and Ö. Hov (1991), Photochemical oxidants in the atmosphere Nord 1991:7, Nordic Council of Ministers, Copenhagen.
- Dlugokencky, E. J., R. C. Myers, P. M. Lang, K. A. Masarie, A. M. Crotwell, K. W. Thoning, B. D. Hall, J. W. Elkins, and L. P. Steele (2005), Conversion of NOAA atmospheric dry air CH<sub>4</sub> mole fractions to a gravimetrically prepared standard scale, *J. Geophys. Res.*, *110*, D18306, doi:10.1029/2005JD006035.
- Eder, B. K., J. M. Davis, and P. Bloomfield (1993), A characterization of the spatiotemporal variability of non-urban ozone concentrations over the eastern United States, *Atmos. Environ.*, *27A*(16), 2645–2668.
- EMEP (2005), *EMEP/CCC-Report 1/2005*, Norwegian Institute for Air Research, Norway.
- Eyring, V., et al. (2007), Multi-model simulations of the impact of international shipping on atmospheric chemistry and climate in 2000 and 2030, *Atmos. Chem. Phys.*, *7*, 757–780.
- Fiore, A. M., D. J. Jacob, B. D. Field, D. G. Streets, S. D. Fernandes, and C. Jang (2002a), Linking air pollution and climate change: The case for controlling methane, *Geophys. Res. Lett.*, *29*(19), 1919, doi:10.1029/2002GL015601.
- Fiore, A. M., D. J. Jacob, I. Bey, R. M. Yantosca, B. D. Field, A. C. Fusco, and J. G. Wilkinson (2002b), Background ozone over the United States in summer: Origin, trend, and contribution to pollution episodes, *J. Geophys. Res.*, *107*(D15), 4275, doi:10.1029/2001JD000982.
- Fiore, A. M., D. J. Jacob, H. Liu, R. M. Yantosca, T. D. Fairlie, and Q. Li (2003), Variability in surface ozone background over the United States: Implications for air quality policy, *J. Geophys. Res.*, *108*(D24), 4787, doi:10.1029/2003JD003855.
- Fiore, A. M., L. W. Horowitz, D. W. Purves, H. Levy II, M. J. Evans, Y. Wang, Q. Li, and R. M. Yantosca (2005), Evaluating the contribution of changes in isoprene emissions to surface ozone trends over the eastern United States, *J. Geophys. Res.*, *110*, D12303, doi:10.1029/2004JD005485.
- Fiore, A. M., L. W. Horowitz, E. J. Dlugokencky, and J. J. West (2006), Impact of meteorology and emissions on methane trends, 1990–2004, *Geophys. Res. Lett.*, *33*, L12809, doi:10.1029/2006GL026199.
- Freidenreich, S. M., and V. Ramaswamy (1999), A new multiple-band solar radiative parameterization for general circulation models, *J. Geophys. Res.*, *104*, 31,389–31,409.
- Geophysical Fluid Dynamics Laboratory (GFDL) Global Atmospheric Model Development Team (GAMDT) (2004), The new GFDL global atmosphere and land model AM2-LM2: Evaluation with prescribed SST simulations, *J. Climate*, *17*, 4641–4673.

- Hansen, J., M. Sato, R. Ruedy, A. Lacis, and V. Oinas (2000), Global warming in the twenty-first century: An alternative scenario, *PNAS* 97, 9875–9880, doi:10.1073/pnas.170278997.
- Henderson, S. C., et al. (1999), Aircraft emissions: Current inventories and future scenarios, in *IPCC Special Report: Aviation and the Global Atmosphere*, edited by J. E. Penner et al., pp. 290–331, Cambridge Univ. Press, New York.
- Horowitz, L. W., et al. (2003), A global simulation of tropospheric ozone and related tracers: Description and evaluation of MOZART, version 2, *J. Geophys. Res.*, 108(D24), 4784, doi:10.1029/2002JD002853.
- Hough, A. M., and R. G. Derwent (1987), Computer modelling studies of the distribution of photochemical ozone production between different hydrocarbons, *Atmos. Environ.*, 21(9), 2015–2033.
- Jacob, D. J., et al. (1993), Simulation of summertime ozone over North America, *J. Geophys. Res.*, 98(D8), 14,797–14,816.
- Kalnay, E., et al. (1996), The NCEP/NCAR 40-year reanalysis project, *Bull. Am. Meteorol. Soc.*, 77, 437–470.
- Kasibhatla, P., et al. (2000), Do emissions from ships have a significant impact on concentrations of nitrogen oxides in the marine boundary layer? *Geophys. Res. Lett.*, 27(15), 2229–2232, doi:10.1029/2000GL011387.
- Lawrence, M. G., P. Jöckel, and R. von Kuhlmann (2001), What does the global mean OH concentration tell us?, *Atmos. Chem. Phys.*, 1, 37–49, www.atmos-chem-phys.org/acp/1/37/.
- Levy, H., II, M. D. Schwarzkopf, L. Horowitz, V. Ramaswamy, and K. L. Findell (2008), Strong sensitivity of late 21st century climate to projected changes in short-lived air pollutants, *J. Geophys. Res.*, 113, D06102, doi:10.1029/2007JD009176.
- Li, Q., et al. (2002), Transatlantic transport of pollution and its effects on surface ozone in Europe and North America, *J. Geophys. Res.*, 107(D13), 4166, doi:10.1029/2001JD001422.
- Liang, J., and M. Z. Jacobson (2000), Effects of subgrid segregation on ozone production efficiency in a chemical model, *Atmos. Environ.*, 34, 2975–2982.
- Logan, J. A. (1989), Ozone in rural areas of the United States, *J. Geophys. Res.*, 94, 8511–8532.
- Marenco, A., H. Gouget, P. Nedelec, J. P. Pages, and F. Karcher (1994), Evidence of a long-term increase in tropospheric ozone from Pic du Midi data series: Consequences: Positive radiative forcing, *J. Geophys. Res.*, 99, 16,617–16,632.
- Martien, P. T., and R. A. Harley (2006), Adjoint sensitivity analysis for a three-dimensional photochemical model: Application to Southern California, *Environ. Sci. Technol.*, 40, 4200–4210.
- Murazaki, K., and P. Hess (2006), How does climate change contribute to surface ozone change over the United States?, *J. Geophys. Res.*, 111, D05301, doi:10.1029/2005JD005873.
- Naik, V., D. Mauzerall, L. Horowitz, M. D. Schwarzkopf, V. Ramaswamy, and M. Oppenheimer (2005), Net radiative forcing due to changes in regional emissions of tropospheric ozone precursors, *J. Geophys. Res.*, 110, D24306, doi:10.1029/2005JD005908.
- Naik, V., D. Mauzerall, L. Horowitz, M. D. Schwarzkopf, V. Ramaswamy, and M. Oppenheimer (2007), On the sensitivity of radiative forcing from biomass burning aerosols and ozone to emission location, *Geophys. Res. Lett.*, 34, L03818, doi:10.1029/2006GL028149.
- Nakicenovic, N., et al. (2000), Special report on emissions scenarios, inter-governmental panel on climate change, p. 599, Cambridge University press, Cambridge, United Kingdom and New York, USA.
- Olivier, J. G. J., A. F. Bouwman, C. W. M. Van der Maas, J. J. M. Berdowski, C. Veldt, J. P. J. Bloos, A. J. H. Visschedijk, P. Y. J. Zandveld, and J. L. Haverlag (1996), Description of EDGAR version 2.0: A set of global emission inventories of greenhouse gases and ozone-depleting substances for all anthropogenic and most natural sources on a per country basis and on 1° × 1° grid. National Institute of Public Health and the Environment (RIVM) report no. 771060 002 / TNO-MEP report no. R96/119.
- Olivier, J. G. J., A. F. Bouwman, J. J. M. Berdowski, C. Veldt, J. P. J. Bloos, A. J. H. Visschedijk, C. W. M. van der Maas, and P. Y. J. Zandveld (1999), Sectoral emission inventories of greenhouse gases for 1990 on a per country basis as well as on 1 × 1 degree, *Environ. Sci. Policy*, 2, 241–264.
- Prather, M. J. (1996), Time scales in atmospheric chemistry: Theory, GWPs for CH<sub>4</sub> and CO, and runaway growth, *Geophys. Res. Lett.*, 23, 2597–2600.
- Prather, M., et al. (2001), in *Climate Change 2001: The Scientific Basis*, edited by J. T. Houghton, Y. Ding, D. J. Griggs, M. Noguer, P. J. van der Linden, X. Dai, K. Maskell, and C. A. Johnson, pp. 239–287, Cambridge University Press, Cambridge.
- Ramaswamy, V., O. Boucher, J. Haigh, D. Hauglustaine, J. Haywood, G. Myhre, T. Nakajima, G. Y. Shi, and S. Solomon (2001), in *Climate Change 2001: The Scientific Basis*, edited by J. T. Houghton, Y. Ding, D. J. Griggs, M. Noguer, P. J. van der Linden, X. Dai, K. Maskell, and C. A. Johnson, pp. 349–416, Cambridge University Press, Cambridge.
- Ravishankara, A. R., E. J. Dunlea, M. A. Blitz, T. J. Dillon, D. E. Heard, M. J. Pilling, R. S. Strekowski, J. M. Nicovich, and P. H. Wine (2002), Redetermination of the rate coefficient for the reaction of O(<sup>1</sup>D) with N<sub>2</sub>, *Geophys. Res. Lett.*, 29(15), 1745, doi:10.1029/2002GL014850.
- Roehl, C. M., et al. (2002), Photodissociation of peroxyacetic acid in the near-IR, *J. Phys. Chem. A and B*, 106(15), 3766–3772.
- Schwarzkopf, M. D., and V. Ramaswamy (1999), Radiative effects of CH<sub>4</sub>, N<sub>2</sub>O, halocarbons and the foreign-broadened H<sub>2</sub>O continuum: A GCM experiment, *J. Geophys. Res.*, 104, 9467–9488.
- Shindell, D. T., G. Faluvegi, N. Bell, and G. A. Schmidt (2005), An emissions-based view of climate forcing by methane and tropospheric ozone, *Geophys. Res. Lett.*, 32, L04803, doi:10.1029/2004GL021900.
- Shindell, D. T., et al. (2006), Multi-model simulations of carbon monoxide: Comparison with observations and projected near-future changes, *J. Geophys. Res.*, 111, D19306, doi:10.1029/2006JD007100.
- Spivakovsky, C. M., et al. (2000), Three-dimensional climatological distribution of tropospheric OH: Update and evaluation, *J. Geophys. Res.*, 105(D7), 8931–8980.
- Sprengnether, M., K. L. Demerjian, N. M. Donahue, and J. G. Anderson (2002), Product analysis of the OH oxidation of isoprene and 1,3-butadiene in the presence of NO, *J. Geophys. Res.*, 107(D15), 4268, doi:10.1029/2001JD000716.
- Stevenson, D. S., et al. (2006), Multi-model ensemble simulations of present-day and near-future tropospheric ozone, *J. Geophys. Res.*, 111, D08301, doi:10.1029/2005JD006338.
- Task Force on Hemispheric Transport of Air Pollution (TF HTAP) (2007), Interim report, available at www.htap.org.
- Van der Werf, G. R., J. T. Randerson, G. J. Collatz, and L. Giglio (2003), Carbon emissions from fires in tropical and subtropical ecosystems, *Global Change Biol.*, 9, 547–562.
- van Noije, T. P. C., et al. (2006), Multi-model ensemble simulations of tropospheric NO<sub>2</sub> compared with GOME retrievals for the year 2000, *Atmos. Chem. Phys.*, 6(10), 2943–2979.
- Wang, Y. H., and D. J. Jacob (1998), Anthropogenic forcing on tropospheric ozone and OH since preindustrial times, *J. Geophys. Res.*, 103, 31,123–31,135.
- Wang, J. S., J. A. Logan, M. B. McElroy, B. N. Duncan, I. A. Megretskaja, and R. M. Yantosca (2004), A 3-D model analysis of the slowdown and interannual variability in the methane growth rate from 1988 to 1997, *Global Biogeochem. Cycles*, 18, GB3011, doi:10.1029/2003GB002180.
- West, J. J., and A. M. Fiore (2005), Management of tropospheric ozone by reducing methane emissions, *Environ. Sci. Technol.*, 39, 4685–4691.
- West, J. J., A. M. Fiore, L. W. Horowitz, and D. L. Mauzerall (2006), Global health benefits of mitigating ozone pollution with methane emission controls, *Proc. Natl. Acad. Sci. U.S.A.*, 103, 3988–3993.
- West, J. J., A. M. Fiore, V. Naik, L. W. Horowitz, M. D. Schwarzkopf, and D. L. Mauzerall (2008), Ozone air quality and radiative forcing consequences of changes in ozone precursor emissions, *Geophys. Res. Lett.*, 34, L06806, doi:10.1029/2006GL029173.
- A. M. Fiore, L. W. Horowitz, and M. D. Schwarzkopf, NOAA Geophysical Fluid Dynamics Laboratory, 201 Forrestal Rd., PO Box 308, Princeton, NJ 08542-0308, USA. (arlene.fiore@noaa.gov)
- V. Naik, Woodrow Wilson School of Public and International Affairs, Princeton University, Princeton, NJ, USA.
- J. J. West, University of North Carolina at Chapel Hill, Chapel Hill, NC, USA.